International Erasmus Mundus Master in
QUATERNARY AND PREHISTORY

WITHIN THE WRIST OF HOMO SAPIENS,
Looking at modularity and sexual dimorphism with a geomorphometry approach on carpal bones

FORAY Charline

Supervisor : Dr. Carlos Lorenzo Merino

Academic year 2023/2024

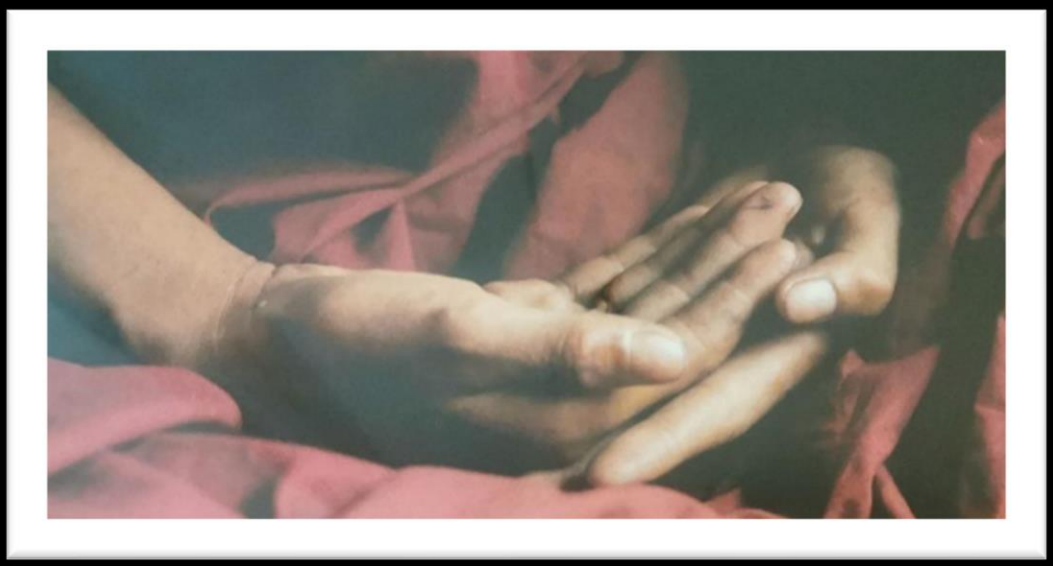

FOREWORD

We cannot go far in the study of the hand, even if we limit ourselves to a mere examination of its surface, before we are forced to notice some facts which bear upon that ever present problem, the question of our own origin (Jones, 1920, p.5)

ACKNOWLEDGEMENT

First and foremost, I would like to express my deep gratitude to my research supervisor, Dr.Carloz Lorenzo Merino, for giving me the opportunity to work in independency, on a consequent collection of bones with high-resolution 3D scanner. He taught me the methodology to carry out the research and I'm grateful for his motivation and sincerity that helps me to level up my ideas into something concrete. I extend my thanks to the CENIEH (Centro Nacional de Investigación sobre la Evolución Humana) working in relation with the Museo de la Evolución Humana in Burgos and the Dr. J.M Carretero for providing us with the opportunity to study the incomparable osteoarchaeological material from the Dominican convent of San Pablo. All of the individuals whose skeletons are now preserved in the collection of the Museum of Burgos were once living beings, and I believe that in the field of palaeoanthropology, it is crucial to keep this in mind. Therefore, I am also grateful to each person whose remains we have excavated. Their bones allow us to explore and answer important questions about humanity.

My completion of this master thesis could not have been accomplished without the great support of my classmates I met during the Erasmus Mundus program. We were there for each other, sharing openly our future projects and engaging in thoughtful discussions about each other's scientific work. It was a privilege to have you all. I address a special thanks to all of them and to the organisation of the Erasmus Mundus program who financially supported my academic life and congress travel I was able to do during both of those academic year.

Since childhood, I've wanted a career in science, and I want to thank my parents, who have supported me every step of the way. They encouraged me to step out of my comfort zone, made it possible for me to travel, and provided a comfortable environment to pursue my goals. Je leur adresse un chaleureux merci. A special thanks to Leïla, my first "second point of view." You not only helped me achieve this master thesis, but you also taught me how to trust myself and my abilities over the past two years. While I was completing this work on my own, a new journey was starting and will continue to unfold for both of us. Trabajando también en tu propia tesis, has estado a mi lado cada día. Por eso, quiero expresarte un agradecimiento muy grande.

ABSTRACT

The wrist has only recently come into the spotlight among scholars thanks to advancements in 2D and 3D imagery analysis since the late 1980s. The development of precise virtual image and a wide range of analytical tools is providing new understanding on wrist function and its complex morphological variation across our Hominin family. For this study, 453 carpal bones from 20 female wrists and 20 male wrists excavated from burials at the San Dominican convent in San Pablo, Burgos (14^{th} and 16^{th} century-dated individuals) were scanned. Here, the central role of virtual anthropology is highlighted by the development of a protocol including every step, from the scanning process and 3D mesh creation to the geomorphometric analysis using landmarks, General Procrustes Analysis. This protocol aims to assess the model that best describes the covariation patterns among the carpals, and also to identify the presence of sexual dimorphism in the population of San Pablo. No significant difference were observed in sexual dimorphism in the population of San Pablo. To our knowledge this is the first time an investigation on modularity has included complete wrists, lacking only the pisiform. Our results indicate that carpals defined as their own modular unit is the best hypothesis to describe covariation patterns within the wrist. Nevertheless, one modular hypothesis based on biomechanical theory showed promising results, suggesting it could be explored further in a broader study. Landmark templates could be expanded to compare Homo sapiens carpals with those of extinct Hominin species.

RESUME

La paléoanthropologie ne s'est intéressée que très récemment à l'étude du poignet dirigée par l'évolution des techniques d'imagerie digitale depuis les années 80. Le développement constant de la précision des images numériques et des outils a permis l'approfondissement des connaissances sur le fonctionnement du poignet et ses variations morphologiques dans l'arbre phylogénétique de notre famille Hominine. Dans cette étude 453 os carpal provenant de 20 poignets de femmes et 20 poignets d'hommes inhumés dans le couvent Dominicain de San Pablo (14^{em} au 16^{em} siècle) à Burgos en Espagne ont été scannés. Le rôle central de la discipline d'anthropologie virtuelle est mise en avant par un protocole incluant les étapes de scanner, de création des mesh 3D jusqu'à leur analyse géomorphometrique à l'aide de landmark et d'analyses Procruste. Ce protocole a pour but d'évaluer le model modulaire décrivant le mieux les schémas de covariation existant entre les os du poignet, ainsi que d'identifier la présence de dimorphisme sexuel au sein des carpal de la population du couvent de San Pablo. Aucune différence significative de dimorphisme sexuel a été observée dans la population de San Pablo. A notre connaissance, c'est la première fois qu'une étude sur la modularité du poignet prend en compte le nombre total des os du poignet excluant seulement le pisiforme. Les résultats indiquent que l'hypothèse selon laquelle chaque os carpal est une unité modulaire à part entière est celle qui décrit le mieux le modèle de covariation des os du poignet. Néanmoins, l'hypothèse fondée sur la théorie biomécanique du « screw-vice model » atteint le second plus haut signal de modularité, suggérant la nécessité d'une étude plus approfondie. Cette étude future pourrait inclure une configuration de landmark encore plus précise ainsi qu'une étude comparé avec les des carpals d'individus Hominines fossiles.

TABLE OF CONTENTS

INDEX OF FIGURES

INDEX OF TABLES

1. INTRODUCTION

The modern human hand is an intriguing blend between primitive and derived trait (Kivell et al., 2022; O.J.Lewis.,1989; Richmond et al., 2016; Tocheri et al., 2008). They differ from those of the non-human primates by their lack of involvement in locomotion behaviour. Indeed, throughout our evolutive history, particularly when we transitioned to fully bipedal beings, our hands started to play crucial roles in exploration, environmental modification, and communication. In that they are recognized as key evolutionary markers for a behavioural transition in fossil hominids locomotion and tool fabrication (Bardo et al., 2017; Bucchi, 2020; Kivell et al., 2022; O.J.Lewis.1989.; Lockwood, 2018.; M. Marzke, 2013; M. W. Marzke, 1971; Richmond et al., 2016; M. Tocheri et al., 2007; M. W. Tocheri et al., 2008).

The first aim of this thesis is to build upon the work of Ana Bucchi et al. (2022) by analysing integration and modular signals inside complete right and left wrists. The protocol applied here is partially similar to hers but includes more data. Indeed, the scanning and multivariate statistical analysis have been expanded to cover all eight carpal bones from left and right hand solely of Homo sapiens, whereas Bucchi's study included multiple species (chimpanzee, gorilla, sapiens), yet on only four carpals from the right hand (capitate, trapezium, lunate, scaphoid). Also, bones scanning was made with equipment that allows more accuracy in 3D mesh, and modifications to the hypotheses were made. Only hypotheses 1 and 8 from Bucchi's work were retained, and six new modular hypotheses were proposed based on surgical and medical literature documenting wrist joints biomechanic models. Those 6 news modular hypothesis resonates with six theories proposed by surgeon and medical individuals who tried since the 19th century to understand carpal bone kinematic and wrist range of motions(Bryce, 1896a; Destot, 2006; Eschweiler et al., 2022; Lichtman et al., 1981; Moritomo et al., 2004; Taleisnik, 1976a).

Then on a second time, presence of sexual dimorphism was also questioned in the sample, as upper limbs were qualified as criterion where sexual dimorphism would be the most accurate specifically within palm and wrist breadth (Barnes et al., 2020; Bennett, 1981; Hiernaux & Hartono, 1980; Loesch et al., 1992).

To sum up we can divide this thesis work into three main objectives :

- **Creation** of a digitalised collection of wrist bones that will be available for the museo of Evolución Humana of Burgos in Spain

- **Conducting** geomorphometric analysis on carpal's cortical surfaces to understand reciprocal interaction between the eight wrist bones and unravelling pattern of shape covariation and modularity for futures comparisons with extinct and extant other Hominoid species.

- **Investigating** sexual dimorphism in carpal bones using shape values from Procrustes coordinates.

2. STATE OF THE ART

As the human hand is known for having greater manipulative ability than any other non-human primates (Bardo et al., 2017, 2020, 2022; Karakostis et al., 2018; Napier, 1956), the wrist has been the subject of extensive paleoanthropological studies aiming to establish quantitively the manual dexterity aspect of Hominids fossils. In order to describe the complex manipulative ability that might be linked with tool making behaviour inside our hominids family, scholars have focused on various aspects, including the efficiency of thumb opposition through examination of both first digit articulation, and scaphoid-trapezium articulation (Bardo et al., 2023; Dunmore et al., 2020, 2023; Morley et al., 2020; M. W. Tocheri, 2007). Additionally, attention has been given to patterns on cortical and trabecular carpal bones (E. Bird et al., 2021; E. E. Bird et al., 2022, 2023; Dunmore et al., 2020; Karakostis & Lorenzo, 2016; Kivell, 2016; Kralick & Tocheri, 2014; Stephens et al., 2018; Syeda et al., 2023; Tsegai et al., 2013), and since the last decades they also conducted analysis on wrist's functionality by investigating biomechanical models and shape covariation study among carpals, arising from the morphometric integration and modularity concepts (Bardo et al., 2023; Bucchi et al., 2022; Galletta et al., 2019a; Morley et al., 2020; C. M. Orr et al., 2010; A.Peña, 2015; M. W. Tocheri, 2007).

2.1.ANATOMY OF THE HAND

The basic morphology humerus-ulna-radius-carpe-metacarpal-phalangeal is present in all mammals and seem to be a very primitive basic trait. The tetrapod's limb is composed by the proximal segment named the **stylopod** connected to the **zeugopod** and then attached to the **autopod**. This basic architecture is known in all limbs of the tetrapod family and are called the **upper arm**, the **forearm** and the **hand**. Although the positional behaviour of the hand inside the members of our super-family Hominoid (genus Homo, Pan, Gorilla, Pongo, Hylobates) is mostly non-bipedal, in this master thesis for the purpose of being understood by all lecturers, we will oriented and described hands with the common anatomical position: The finger pointing down and the palm facing forward. Below is a list of additional directional anatomical terms (Figure 1).

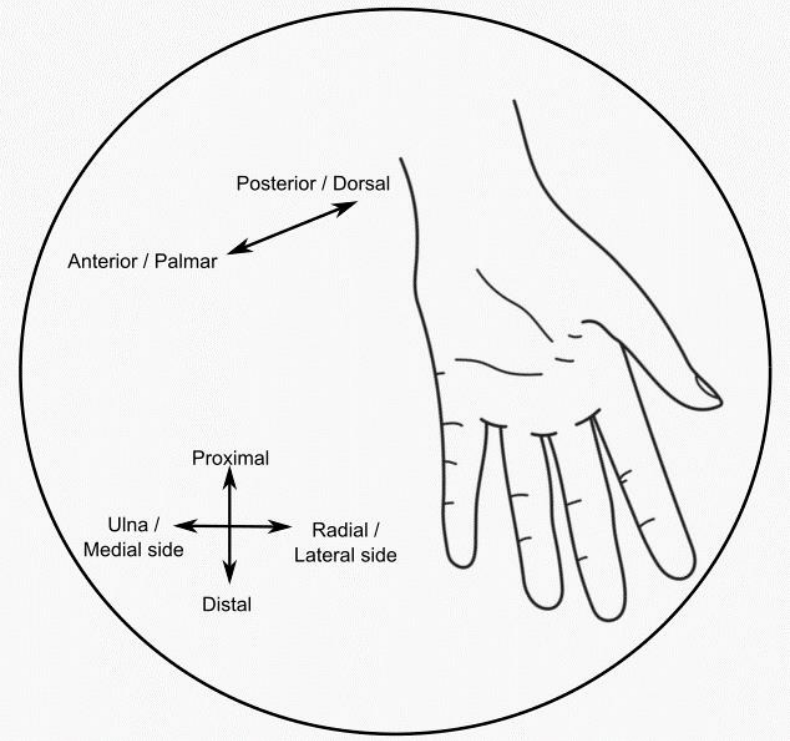

Figure 1: directional anatomical terms

- ☞ The wrist : proximal part
- ☞ The finger : distal part.
- ☞ The palm : anterior side
- ☞ The dorsal surface or back of the hand : posterior side
- ☞ The fifth finger : the medial side or ulna side
- ☞ The thumb : the lateral side or radial side
- ☞ Palm up = supination movement
- ☞ Palm down = pronation movement

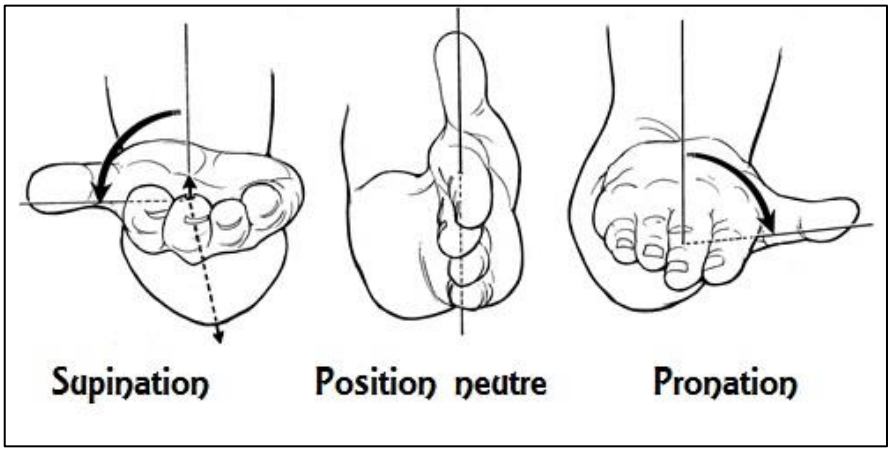

Figure 2: range of motion of the wrist

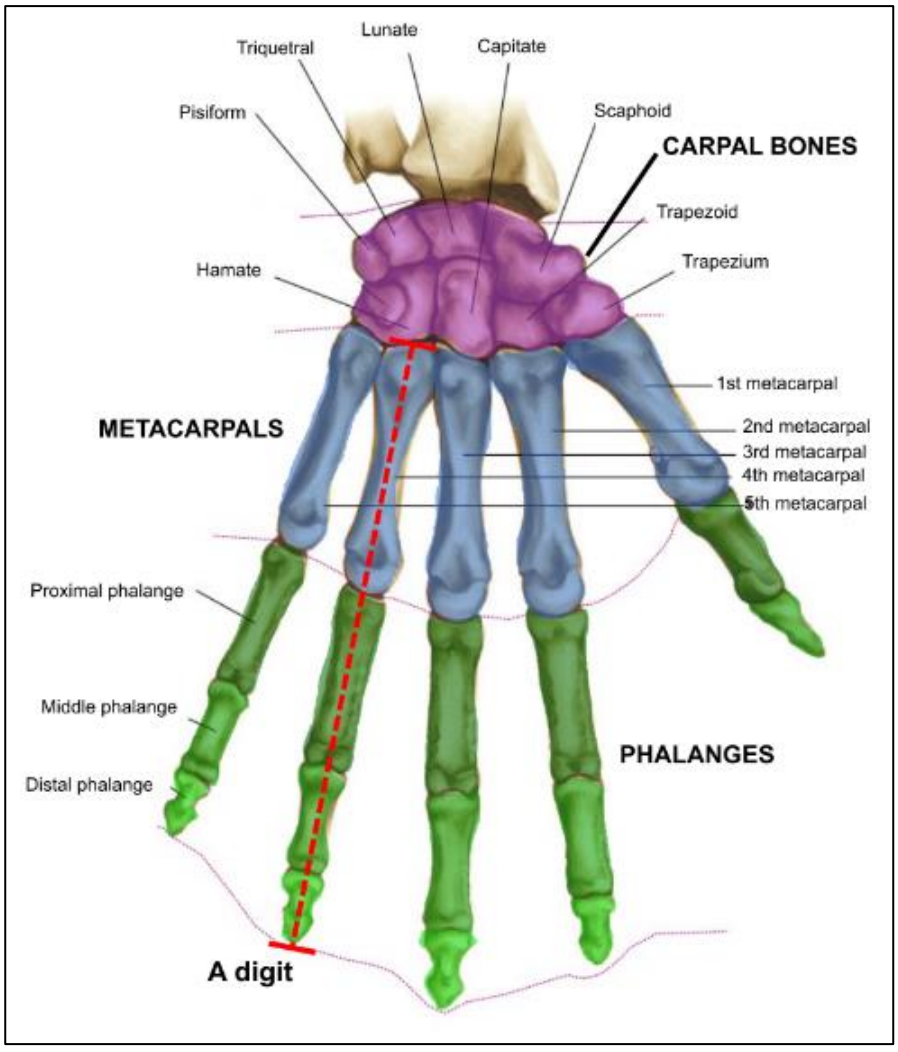

Figure 3: osteology of the hand

27 bones formed the hominoid hand. This is one of the largest group in the human skeleton. We usually divide them into 3 groups, so as proximally to distally : The 8 carpals (wrist bones), the 5 metacarpals and the 14 phalangeal. The mains parts of our hand are, our 4 fingers, our thumb that can move independently with a wide range of movement, the palmar surface and our wrist. We call “a digit” the alignment of a metacarpal that articulates with a proximal phalange (PP), than with an intermediate/medial phalange (MP) and finally a distal phalange (DP), except for the thumb that doesn’t have intermediate phalangeal (Figure 3). Both metacarpal and phalanges are long bones with a semi-circular shaft and a condyloid distal head. Metacarpal’s distal head have the most condyloid shape to articulates with the concave base of the proximal phalanges. Same is seen with the distal head of the proximal phalanges and middle phalanges, while distal phalanges are easily to distinguished by their expand apical tufts at their distal ends. Our forearm is connected with our hand by the wrist. It is a collection of articulation between eight carpal bones with high complexity joints and interosseous kinematic.

The carpal complex provides the hand with a wide hemisphere of circumduction (Figure 2). It is composed by 8 carpal bones with distinctive morphology and irregular shape with various side. They are usually divided into 2 rows (Figure 4) :

- The proximal row (ulnar to radial side) : pisiform, triquetral, lunate, scaphoid
- The distal row (ulnar to radial side) : hamate, capitate, trapezoid, trapezium

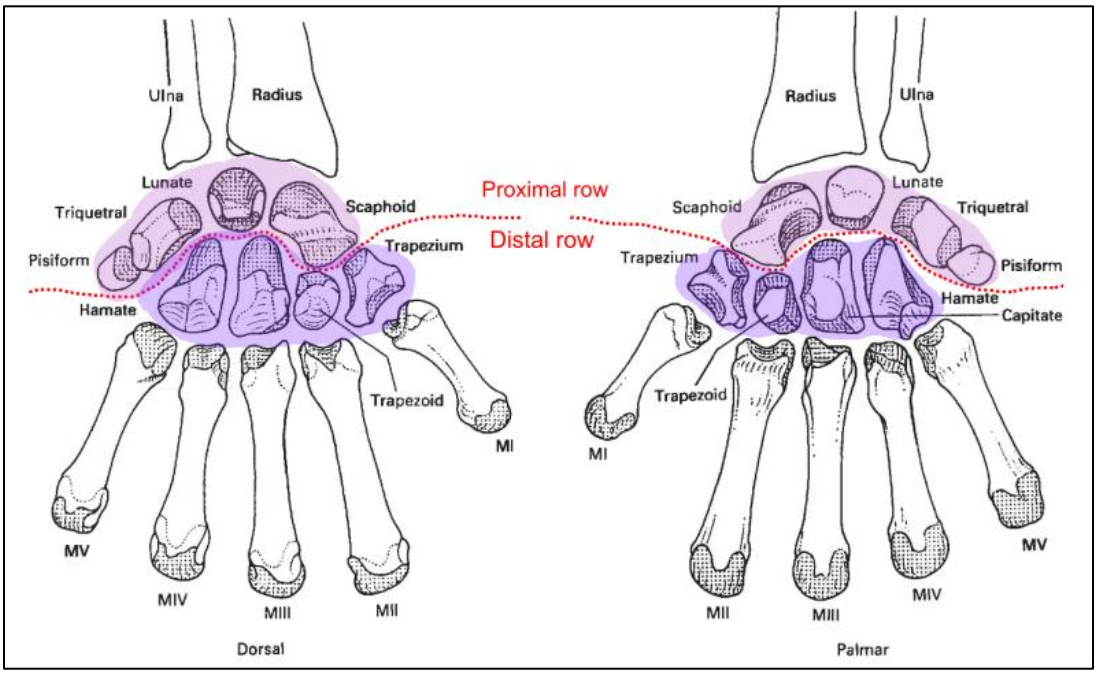

Figure 4: osteology of the wrist, modified from L. Aiello & C. Dean (1990)

Carpal bones don't have entheses but are surrounded by a dense cartilaginous surface with numerous ligaments. We usually divide the ligaments into two groups : **ligaments extraneous** that origins on the ulnar or radius and inserts deeper in the hand skeleton, and **the ligaments intraosseous** that originates and insert inside the wrist. They maintain stable the carpal by keeping them bonded all together and allowing the pluriaxis and pluridirectional movement of the wrist (most importantly the scapholunate et the lunotriquetral ligaments). Medial nerves and nine tendons pass through the wrist inside the **carpal tunnel**, then reach fingers and other parts of the hand. It is formed by the concave shape of the carpal bones and the flexor retinaculum (a roof-like fibrous band over the carpal on the palmar side). The **intrinsic muscles** that origin and insert inside the hands allow fine motor movements (pinch, grip, thumb movement) and **extrinsic muscles** that origin outside of the hand skeleton are responsible for hand's strength.

Scholars have conducted various studies on the **wrist joints** of extinct and present-day hominoids, examining loading distribution, as well as the morphology of proximal carpals and the orientation of facets, to assess potential effects of stone tool manufacturing on bones' shape variation (Bucchi, 2020; Bucchi et al., 2022; C. Orr et al., 2023; Tencer et al., 1988). **The radiocarpal joint** has the proximal row of carpal and the distal end of the radius connected together on a convex triangular surface made of fibrocartilage : scaphoid and lunate articulates with the radius. The **midcarpal synovial joints** is connecting the proximal row of carpals from the distal one and facilitating the continuous movement started at the radiocarpal articulation : scaphoid articulates with the trapezium and trapezoid and capitate ; lunate articulates with the capitate ; triquetral articulates with the hamate. On the **Carpometacarpal joints** the proximal head of each metacarpal articulates with one of a distal row's carpal : trapezium with Mc1 ; trapezoid with Mc3 ; capitate with Mc3; hamate with Mc 4 et 5. The distinct saddle-shape of the trapezium-MC1 articulation surface has been the most carpometacarpal joints studied this far (Bardo et al., 2020, 2023; Bucchi, 2020; Dunmore et al., 2023; Galletta et al., 2019b; Kivell, 2021, 2021; M. W. Tocheri, 2007). It makes sense to remind that the thumb is a relevant features used to define us in the family of apes "*capable not only of the power grip but also of the precision grip as defined by Napier in 1956"*(Bucchi, 2020). The unique concave facet of this carpometacarpal joints at the edge of the radial side have remarkably influence thumb mobility strength and manual abilities. The fourth others carpometacarpal joints have less range motion in term of Adduction/Abduction and Flexion/Extension movement.

2.2.BONE DEVELOPMENT OF THE HAND

The hand architecture is regulated by the expression of Hoxd genes, a subgroup of the HOX genes known as "homeotic genes," which are responsible for establishing body axis polarity early in embryonic development (Tarchini & Duboule, 2006). The Hoxd genes control the development and ossification of fingers (Garrec, 2008), which begins prenatally, and continue all through puberty. However, carpals are observed later after birth (Gaskin et al., 2011; Gilsanz & Ratib, 2005) and appears in an order that doesn't follow a general proximal to distal evolution (Figure 5). The actors and factors responsible for wrist development have not yet been fully identified. Only a few studies have been conducted, and they have not produced conclusive results, revealing only a complex mechanism with many unanswered questions.

Fidel Hita-Contreras and her colleagues have developed a temporal-spatial sequence of the emergence and development of ligaments, fibrocartilaginous structures, and neuro-muscular elements in the embryonic region (Hita-Contreras et al., 2012). They observed immature cartilage structures in the following chronology : the capitate (embryony stage 20), then scaphoid, lunate, hamate, triquetrum (stage 21), and trapezium, trapezoid, pisiform (stage 22). At birth, we can observe all metacarpals and phalanges diaphysis but no carpal. Longitudinal growth in the metacarpals and phalanges initially occurs in their shafts at the primary centres of ossification. After birth, until around the age of 15, secondary ossification centres (epiphyses) form and grow until they fuse with the diaphysis. In contrast, the carpal bones ossify entirely from their primary centres after birth and do not have epiphyses. There is an established sequence of ossification (Gaskin et al., 2011; Gilsanz & Ratib, 2005) : capitate - hamate - triquetral - lunate - trapezium - trapezoid - scaphoid – pisiform (Figure 6). Comparing with the temporal-spatial sequence of immature cartilage structures appearance in embryo, we can note that only scaphoid ossifies after trapezium and trapezoid yet its cartilage fibrous are observed before theirs.

Below is a bone developmental growth sequence based on radiography observations from a new born to a young teenager's hand skeleton (Gaskin et al., 2011; Gilsanz & Ratib, 2005). It is wised to note that medical research has showed a difference in the bone development chronology between sexes. Indeed, in female individual bone growth is faster and age maturity.

appear earlier than in male individual (female hand's skeleton growth is completed at 13-14yo). The following figure shows a bone growth development sequence of a male hand's skeleton.

Figure 5: hand bones development

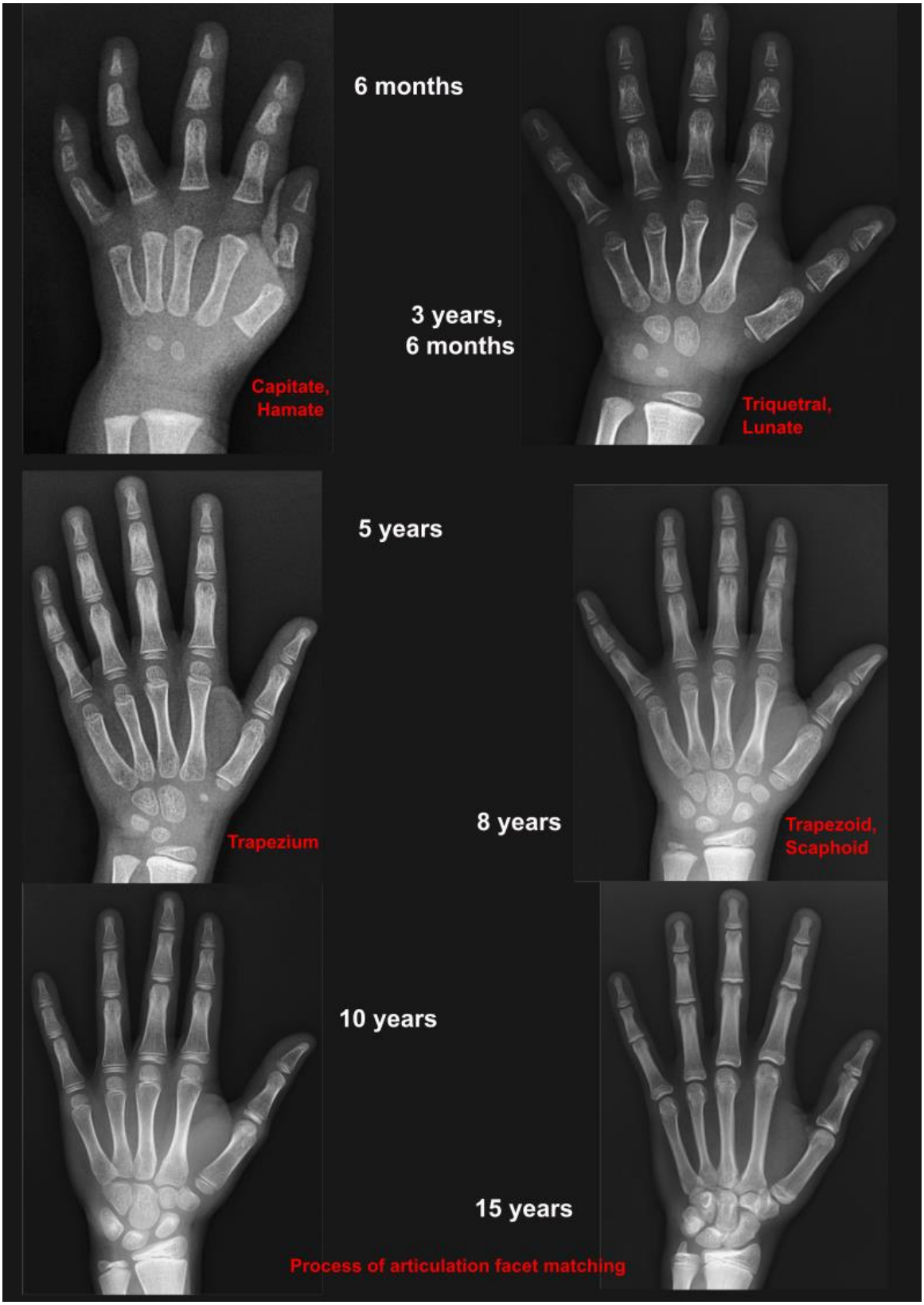

Figure 6: hands X-ray pictures of child from 0 to 15 yo

2.3.THEORIES AND MODELS OF WRIST BIOMECHANIC

The high complexity of articulations and dense network of ligaments in the wrist make it particularly challenging to understand carpal kinematics. Since the first dissections on cadavers, numerous models and theories on the biomechanics of the wrist (Figure 7) have been proposed over time, to elucidate its wide range of motions. These have been based on anatomical dissection, radiography, and later imaging techniques such as CT scans and magnetic resonance imaging (Bryce, 1896; Eschweiler et al., 2022; Kamal et al., 2016; Lichtman et al., 1981; MacConaill, 1941; Moritomo et al., 2004; Rohde et al., 2010; Taleisnik, 1976). The following theories have influenced the proposed a priori hypothesis for the modularity test of this thesis work (Table 5)

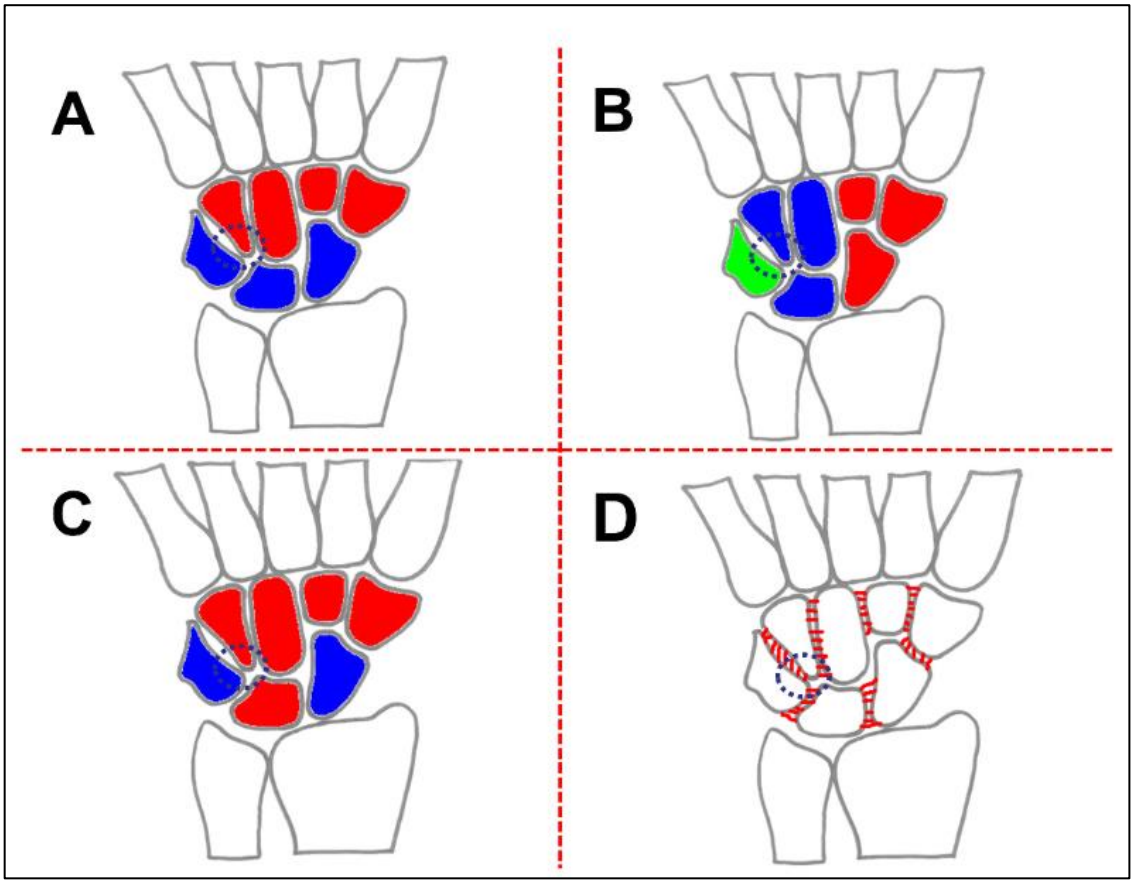

Figure 7: illustration of wrist kinematic theory modified from J. Eschweiler (2022), ***(A)*** *Row-theory,* ***(B)*** *Column-theory,* ***(C)*** *Row-Column theory,* ***(D)*** *Ring model*

- *the Row theory* (1896) (Figure 7 A)

Right after the radiography was developed by Roentgen, Bryce conducted radiographic observation on normal subject to describe carpal motion (Bryce, 1896b). In the mean time, Etienne Destot highlighted the importance of the scapholunate ligament in charge of stabilisation of the PCR in his radiographic work at l'Hotel Dieu in Lyon, France (Destot, 2006). They advocate the traditional cluster : a division into 2 horizontal rows, the proximal and the distal rows (respectively PCR and DCR).

- *Column theory* (1921) (Figure 7 B)

Navarro propose the existence of a radial, central, and ulnar column in the wrist. He divides the carpus complex into the scaphoid trapezium and trapezoid in one column in charge of wrist mobility, the capitate lunate and hamate in the central column in charge of flexion/extension movement, and the triquetral with pisiform in the ulnar column in charge of the rotatory movement (Eschweiler et al., 2022).

- *Row Column theory* (1976) (Figure 7 C)

Fifty years after Navarro's model Taleisnik adapted the "column theory" by gathering the lunate capitate hamate trapezoid and trapezium into one central column, and isolating the scaphoid and the triquetral in their individual column. He named the central column a "T-structure" in charge of flexion / extension movement, and attributed the role to the scaphoid as a stabilisation link in the midcarpal joint. The triquetral is a pivot for wrist rotation movement (Taleisnik, 1976b).

- *Ring model* (1981) (Figure 7 D)

Lichtman and his colleagues investigated on cadaver and clinical examination wrist composition and described what they called the ring model. It implies two mobile links in the carpus. They identify the mobile trapezioscaphoid articulation and the rotatory triquetrohamate articulation with the helicoidal shape of joint(Lichtman et al., 1981). With this models they expose the motion behaviour such as : "movement by one row is in the opposite direction from that by the other"(Eschweiler et al., 2022, p. 10).

- *Screw Vice or Clamp-Theory* (1941) (Figure 8)

MacConail published his theory after his investigation on one cadaver. He observes that in dorsiflexion the carpus are bended together thanks to a two stage process : " The first stage of dorsiflexion is, then, one in which the clamp is set up, or constituted, by fixing the navicular, the fixed jaw of the vice, to the distal row, which acts mechanically as the base of the vice. In the second stage, the hamate acts as a screw to pin the lunate against the fixed jaw, and to hold it there for so long as dorsiflexion is maintained" (MacConaill, 1941, p. 6). He described the carpus as a units with three masses (Figure 8) : the scaphoid on itself forms the first one, the lunate and triquetral form the second one, and a third distal structures formed by the hamate capitate and trapezoid. His separation of the scaphoid from others carpal bones is based upon the observed fact that this bone moves at a times with the PCR and at times with the DCR (MacConaill, 1941).

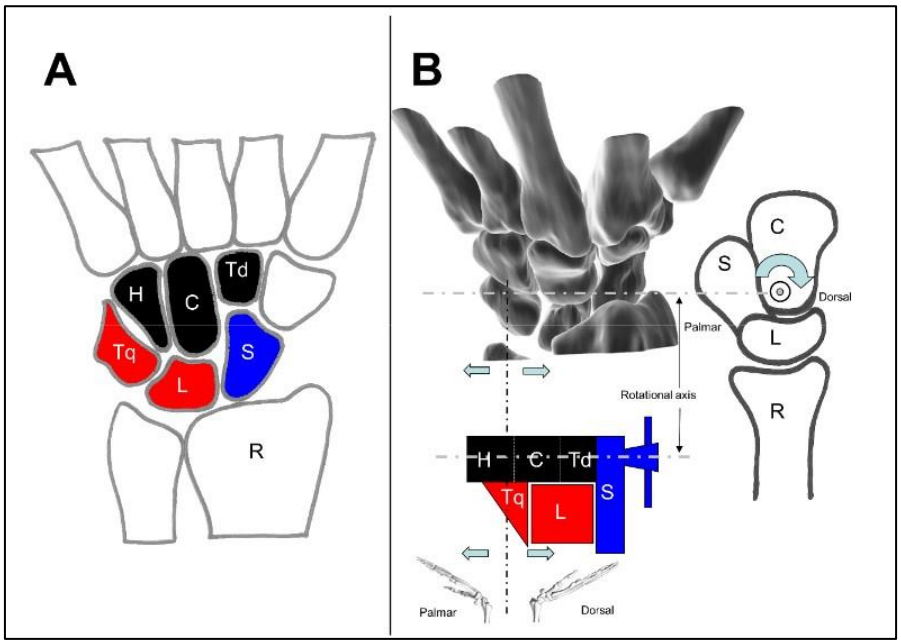

Figure 8: Screw-vice or Clamp model, modified from J. Eschweiler (2022)

- *Ovoid model or C-shape concept* (2006) (Figure 9)

Moritomo and his colleagues studied *in-vivo* kinematic of the mid-carpal joint with high accuracy imagery technology (MRI) in the University Medical School of Osaka, Japan. They display the carpus structure in an ovoid volume or a "C-shaped"(Figure 9). They postulated that midcarpal motion is the combination of 3 types of joints : the scaphoid with the distal row (uniaxial) , lunate triquetrum and distal row (biaxial and ellipsoidal), intercarpal joint of the

PCR. Moritomo et al use the Ovoid / C-shape to explain the carpal self stabilizing mechanism (Moritomo et al., 2004).

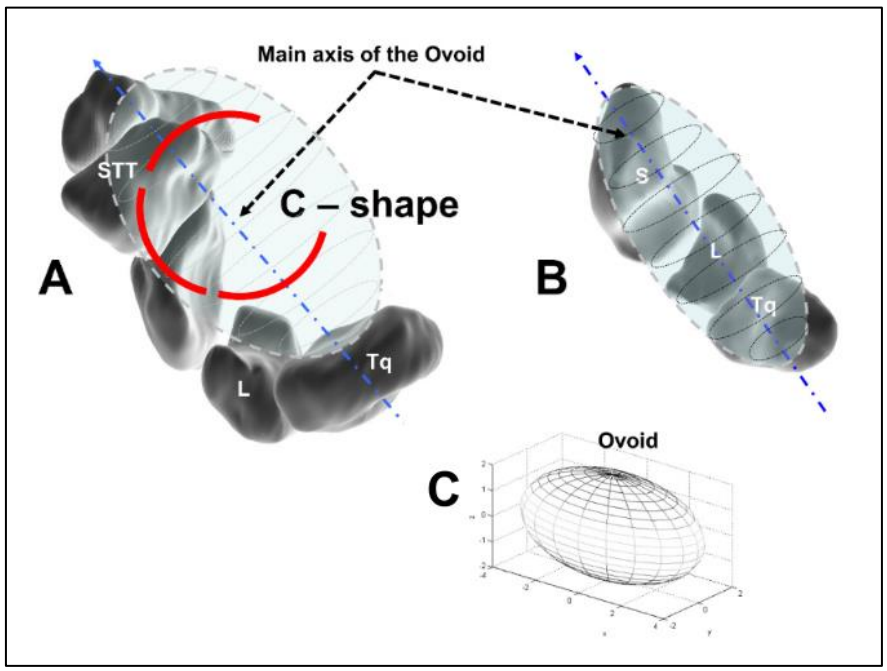

Figure 9: modified from J. Eschweiler (2022), C-shape or Ovoid model

2.4. VIRTUAL ANTHROPOLOGY BACKGROUND

The exponential growth and integration of three-dimensional imaging technologies, into paleoanthropological fields of research.

"Virtual anthropology" is best described as a multidisciplinary and interdisciplinary approach to investigate anatomical data with 3D representation of especially the human species its lineage and closest relatives' primates. This young discipline (The first 3D image created from high resolution 2 dimensions serial computed tomographic scan data was done in 1986 (Conroy & Vannier, 1984)) is made up of a pool of different domains such as anthropology, primatology, medicine, palaeontology, as well as mathematics, statistics, and digital technologies. It has been divided into 6 main work areas (Gerhard W.Weber & Fred L.Bookstein, 2010): **Digitise** ; **Compare** ; **Reconstruct** ; **Expose** ; **Materialise** ; and **Share**. The ability to look inside anatomical objects stemmed from the late discovery of X-rays, initially used for radiology in the early 20th century. The curiosity to explore the interior of a fossilized skull was finally satisfied in 1906 when a team of German paleoanthropologists utilized computed tomography

scans on a Neanderthal individual from Croatia (Gorjanović-Kramberger, 1906).However they were still not capable of taking out the sediment matrix. When Godfrey Neu-bold Hounsflied discovered how to create a virtual image in 3 dimensions by associating X-ray application with computer technology, it becomes a revolutionary tool for paleoanatomist(Taquet, 2010). The technic called computed tomography (named later in the text CT) has never stopped to improve since then (Figure 10). Nowadays many new applications have emerged, alongside the development of increasingly advanced 3D imaging tools and software.

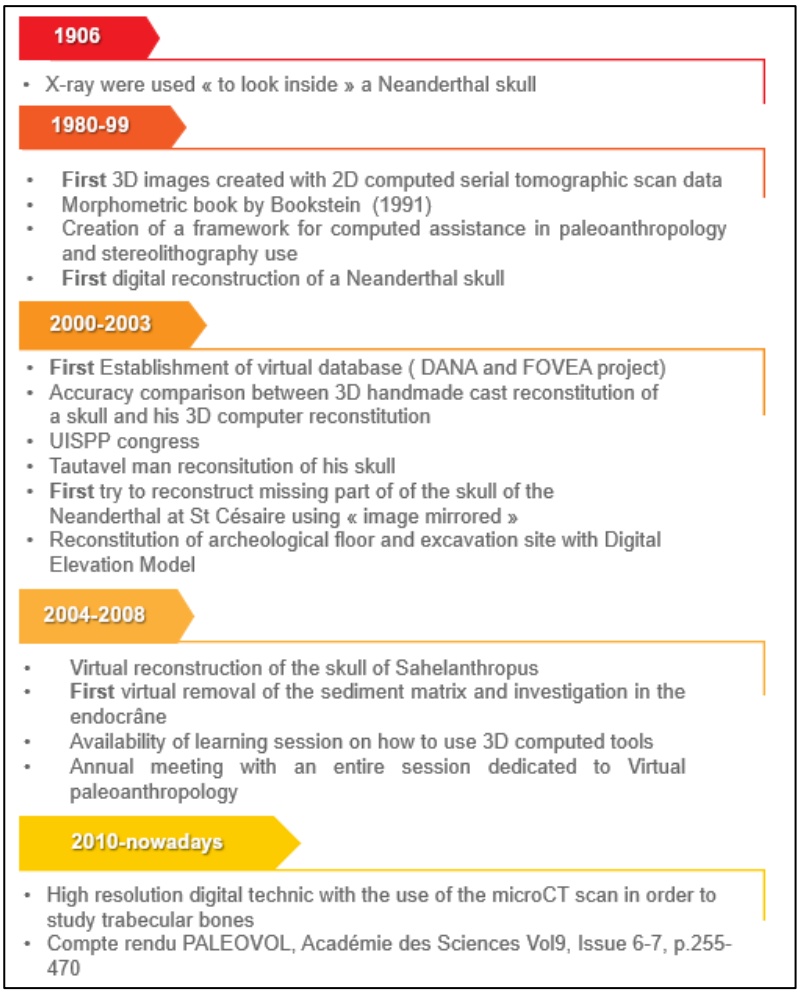

Figure 10: Chronological history of the virtual anthropology discipline

Each of these applications has its own characteristics, offering varying levels of image resolution depending on their price and the researchers' ability to use them independently. For example, photogrammetric modelling is a low-cost option for creating 3D models of artifact surfaces, with user-friendly image processing software (Sumner & Riddle, 2008). On the other hand, synchrotron scanners, which use magnetic resonance imaging, provide exceptionally high-resolution scans of artifact interiors using X-ray projection. However, synchrotron

facilities are costly to use and require skilled technicians to assist researchers (Ponce de León et al., 2021). Despite the extreme differences between these two techniques, they both cover every step of the process, from digitizing the artifact for morphometric calculations and statistical analysis, to storing it in a shared virtual database. Additionally, for heritage accessibility, these techniques can lead to the creation of 3D printed models. Nowadays, digital applications are increasingly common among medical scientists, anthropologists, and heritage conservation researchers. The popularity of 3D surface scanners is driven by their easy availability, affordable prices, and the development of user-friendly software, some of which are even free. In conclusion we can see significant benefits in term of accessibility (first digital database creation initiative dated back in the beginning of our 21st century with de DANA American project and the FOVEA European project (Clark et al., 2001; Guipert et al., 2003)), improvement of digital modification and manipulative ability erase deterioration concern as well as government restriction and travel cost. Undeniably "virtual anthropology" lead to new paleoanthropological interpretations, new perspectives for the conservations area and finally new possibilities for museography displays.

Although CT scanning technic allows paleoanthropologist to explore fossils hominids internal features in a non-invasive way, scholars that are using daily this technology are raising some issues and methodology aspects that need to be discussed and highlighted to guarantee an intemporal optimal scientific exploitations.

Firstly, "paleotomography" (term used by Gaël Clément Didier and Geffard-Kuriyama in CR Palevol Volume 9, Issues 6–7, 2010, p. 255-257) application sometimes bumped into informatic limits when maximum resolution is required but computer calculation capacity are unable to handle it, as well as the limited storage place and the time needed for uploading the high resolution images. Moreover, as software becomes increasingly complex with amplifying possibilities, scholars will need complementary knowledge on informatic and imaging methodology otherwise a lost in protocol's accuracy could happen. We know that "different sources of uncertainty are involved at each step of the complete procedure when imaging methodologies are exploited […]"(Balzeau et al., 2010) leading to a loss of explanation of metric landmark determination or informatic treatment in the methodology section of scientific articles. Then, from another aspect of "virtual palaeoanthropology", Antoine Balzeau and his colleagues expose today difficulty in getting access to virtual database and issues about ownership of this digital data. Is the person who made the scan the owners of the 3D images ? Is it the same owners that is in charge of the CT scan images, the 3D images, and the printed 3D model ? Antoine balzeau and his colleagues propose a guideline for "[…]the preservation,

management and development of collections while preserving their scientific exploitation"(Balzeau et al., 2010,p272).

In 2010, the Compte Rendu PALEOVOL Volume 9, Issues 6–7, Pages 255-470, titled "Imaging & 3D in palaeontology and palaeoanthropology" edited by Gaël Clément and Didier Geffard-Kuriyama, provided an overview of various imaging techniques such as 2D slices, computed image scanning, and 3D virtual reconstruction used in the fields of palaeontology and palaeoanthropology. It emphasized that while these visualization and analysis methods are valuable, they should not replace the study of original fossils but rather be seen as additional tools. A decade later, we continue to utilize both these methodologies. However, the emergence of machine learning and artificial intelligence has enabled us to access increasingly precise, faster, and deeper insights into prehistoric research(Abdelhady et al., 2024).

2.5.GEOMETRY MORPHOMETRY APPROACH

Since the 1980s, there has been a significant increase in the use of numerical methods in the fields of palaeontology and prehistory. Geometric morphometric techniques are among these advancements. They allow to separate size from the shape (Figure 11) and so that comparison study can be done by isolating, reducing or even deleting the effect of size on digitals specimens.

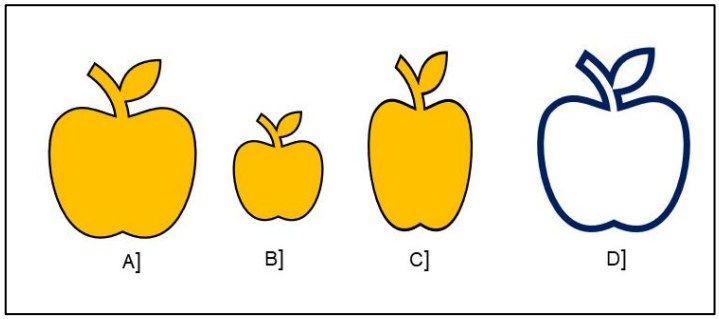

*Figure 11: illustration of size and shape, **[A]** and **[B]** have the same shape but not the same size, **[A]** and **[C]** have the same size but not the same shape, and **[D]** have the same shape and size but not the same colour as **[A]***

Landmark-based morphometric studies are a primary application of these techniques, offering the advantage of easily visualized and interpreted results. In this master's thesis, we investigate the interrelation between the shapes of wrist bones by recording geometric locations of landmark points.

A landmark is defined as “discrete points that correspond among all the forms of a data set” (Bookstein, 1991, p. 58). These points can be located in either a 3D or a 2D space. There are two main classifications of landmarks:

The first one is from Dryden & Maria (1998) :

- **Anatomical landmarks** are homologous point that can be found on all specimen of the study .
- **Mathematical landmarks** are points defined on the basis of some geometry property (maximum of curvature, end of the bones)
- **Pseudo-landmarks** are spaced points well localised between two anatomical or mathematical landmarks.

Another classification was made by Bookstein (1991) :

- **Landmark of Type I** are localised where tissues or bones meet.
- **Landmark of Types II** are defined by local property such as maximal/minimal curvature.
- **Landmark of Type III** are localised at extreme position, or at constructed points such as centroids.

Geometric morphometric study is the analysis of coordinates of a set of landmarks on a number of specimens. However, when landmarks are digitalized it is impossible to ensure that all specimens had the same position and same orientation. Consequently, if we want to compare shape with or without the variable of size, we need to go through a process of translation and rotation of specimen and standardization of the coordinates position and orientation. Bookstein (1984), proposed to take 2 landmarks in the set and use them to create a baseline so that Landmark 1 has the coordinates (0,0) and Landmark 2 (0,1). All landmarks registered in this new baseline constitute what is called “ **the Bookstein coordinates** of the shape” (Figure 12).

> *“Figure 5.1.3 shows three sets of shape coordinates for the same scalene triangle: The coordinate of A to baseline BC, the coordinates of B to baseline AC, and the coordinates of C to baseline AB are all different. There are likewise three other sets of shape coordinates corresponding to the same baselines taken with reversed sense. These shape coordinates-^ to baseline CB, B to baseline C4, and C to baseline BA - correspond to a rotation of the first group by 180° around the point (0.5,0), the centre of the baseline. This midpoint will be encountered again in connection with size-shape covariances”*

(Bookstein, 1991, p. 130)

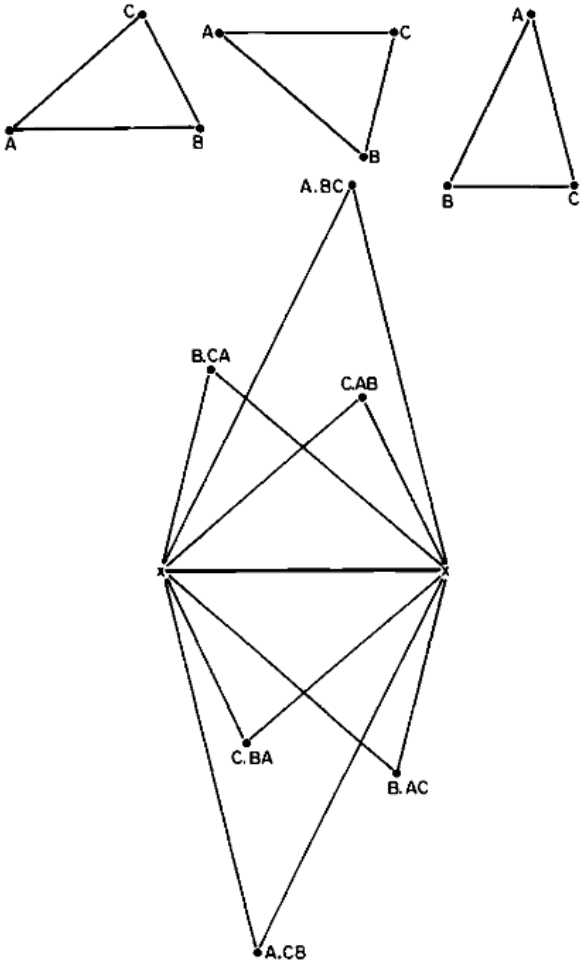

5.1.2. Change of baseline

Figure 5.1.3. Six sets of shape coordinates: the same triangle *ABC* to six different baselines. Notation: *A.BC*, shape coordinates of point *A* to a baseline from *B* to *C*, and similarly the others.

Figure 12: Shape coordinates from a baseline proposed by Bookstein, modified from Bookstein (1991)

However, this technic creates a fixed positions, and landmarks close to the baseline will get smaller variance between objects of the sample (Bookstein, 1991; Hammer & Harper, 2006). Thus, the common approach, also the one used in this master thesis, is minimizing the total sum of squared distances between corresponding landmarks. It is called Procrustes fitting (Figure 13).

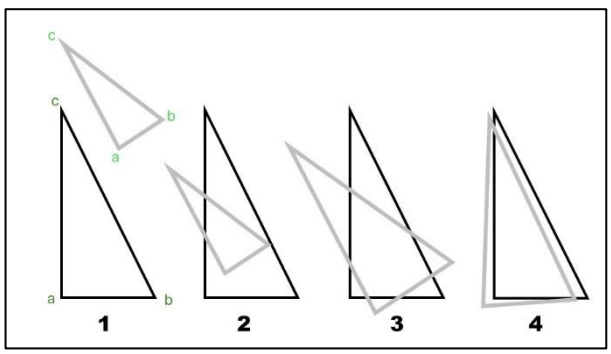

Figure 13: illustration modified from Julie Arnaud class of the Procrustes fitting process with three coordinates points of a triangle (a, b, c)

Least-squares or Procrustes fitting algorithm is scaling, rotating, and translating the sets of landmarks in order to have them into standardized size, orientation and position before further investigations (Figure 13). We call landmarks coordinates resulting from Procrustes fitting " Procrustes coordinates". In this master thesis, we conducted full Procrustes fit on landmarks coordinates of carpal bones deleting size effect and leaving only shape for comparison. The full General Procrustes Analysis were conducted to approach shape variation on carpals.

2.6. MORPHOLOGICAL INTEGRATION AND MODULARITY

The concept of morphological integration originates from the early days of biology as a science, particularly through the work of Georges Cuvier (1982) in comparative anatomy. This concept has been applied at various levels, including genetic and environmental studies, ecological interactions (Klingenberg, 2008, 2009, 2013, 2014), and even evolutionary developmental sciences. Olson and Miller's groundbreaking book, *Morphological Integration* (Olson and Miller, 1985), elevated this concept to the forefront of phenotypic studies. Modularity, a general characteristic observed in biology, has also been extended to a wide range of diverse fields such as architecture and design, social sciences, and transportation. Both concepts are closely connected and explain how different traits within a structure are more or less correlated (Goswami & Polly, 2010): "*Integration is the tendency of different traits to vary jointly, in a coordinated manner, throughout a morphological structure or even a whole organism*" (Klingenberg, 2014, p. 2). Traits exist within a module, which is highly integrated by numerous and strong interactions, while different modules are connected by few and weak interactions (Klingenberg, 2008). Consequently, modularity reflects the high level of integration within specific parts or regions of a structure, known as modules, but indicates weak integration between these modules. "[Morphological modularity] *means that integration in a structure is compartmentalized, with strong within-module and weak between-module integration*" (Klingenberg, 2014, p. 2). The strength of covariation is the main criterion for assessing modularity in morphometric data. Analysing modularity within the wrist can highlight suspensory locomotion specificity, manual ability, and phylogenetic evolution evidence. Indeed, A. Peña used geometric morphometric techniques to study integration and modularity in the wrist of hominoids (Peña, 2018). She examined how covariation patterns may have shaped the evolution of wrist structures in primates. Her research, along with studies testing

modular organization in the wrists of modern humans, chimpanzees, and gorillas (Bucchi et al., 2022; Williams, 2010), and the morpho-functional characteristics of the thumb and radial side of the wrist as indicators of tool-related behaviour in human and Neanderthal hands (Bardo et al., 2020), have significantly advanced our understanding in this field.

To apply the concept of modularity to biological problems, we require a specific context that defines morphological modules within our structure. By subdividing the total set of traits into modules, we can compare covariation between these modules to examine the strength and number of integrations. This allows the evaluation of modularity within morphological elements (Klingenberg, 2008). By studying the covariation of traits within the carpal complex as cohesive units, we can evaluate integration between structures and define functional modules within the skeletal system of the wrist (Bardo et al., 2020; Bucchi et al., 2022; Peña, 2018). In short, we are looking for a modular configuration that fit best the covariation patterns that exist within the wrist.

3. PALEOANTHROPOLOGICAL MATERIAL

This thesis work, host a consequent sample of 453 carpal bones belonging to 40 individuals from a population of 50 individuals (25 females and 25 males) who lived between the 12th and 13th century in Burgos, Spain. Their burial were excavated in the early years 2000. Although it belongs to the museo de la Evolución Humana of Burgos in Spain and its investigation centre the CENIEH, it was stored in the office of palaeoanthropology of the institute of paleoecology Humana i Evolucion social de Tarragona (IPHES) in Catalunya. Numerisation equipment were used there in order to scan them and create a digital 3D collection.

3.1. THE DOMINICAN CONVENT OF BURGOS

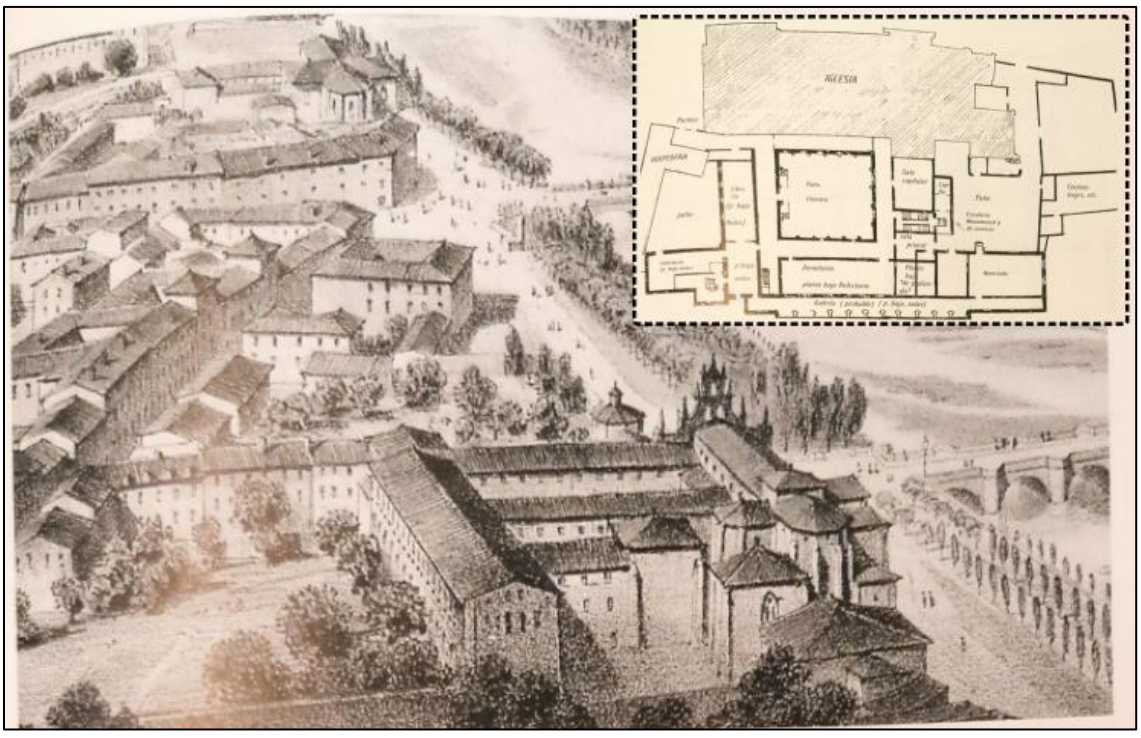

*Figure 14: The Dominican convent in the 13th century from the East, **Up right** distribution of the dependence of the convent ©J.A Casilla Garcia & Gema Adan Alvarez (2005)*

The collection used in this thesis is coming from the cemetery of an ancient Dominican convent (Figure 14) founded by an influential priest named Santo Domingo de Guzman. Thanks to the protection of the kings and financial input from high stature people, Dominican preachers built on the beginning of the Thirteen century "The Convento dominico de San Pablo" in the city of

Burgos in north of Spain (*42.39260774642961, -3.682347641025585*). During this period of time known by historian as flourishing for the Dominican orders, they were able to move from a primitive monastery outside of the city and established their convent inside it. It became a central hub for the people of Burgos, offering services like a library, hospital dormitory, and refectory. The influence of the Dominican order extended to politics and culture in the region. After six prosperous centuries, the Dominican legacy faced challenges during the French invasion when the convent was repurposed as a prison, military hospital, and military deposit in the beginning of the nineteenth century. Although some parts of the building were occasionally used by remaining Dominican priests, they were eventually expelled. By the time of 1850, the convent properties were exploited, stolen, and much of the stone structure ruins was reused. Over six centuries, this place played a vital role in the lives of the people in the region of SP. Before embarking on the construction of the future "Museo de la Evolution Humana" (Figure 15) they decided to conduct an excavation to document the history and archaeological objects left behind in the ancient convent (Figure 16).

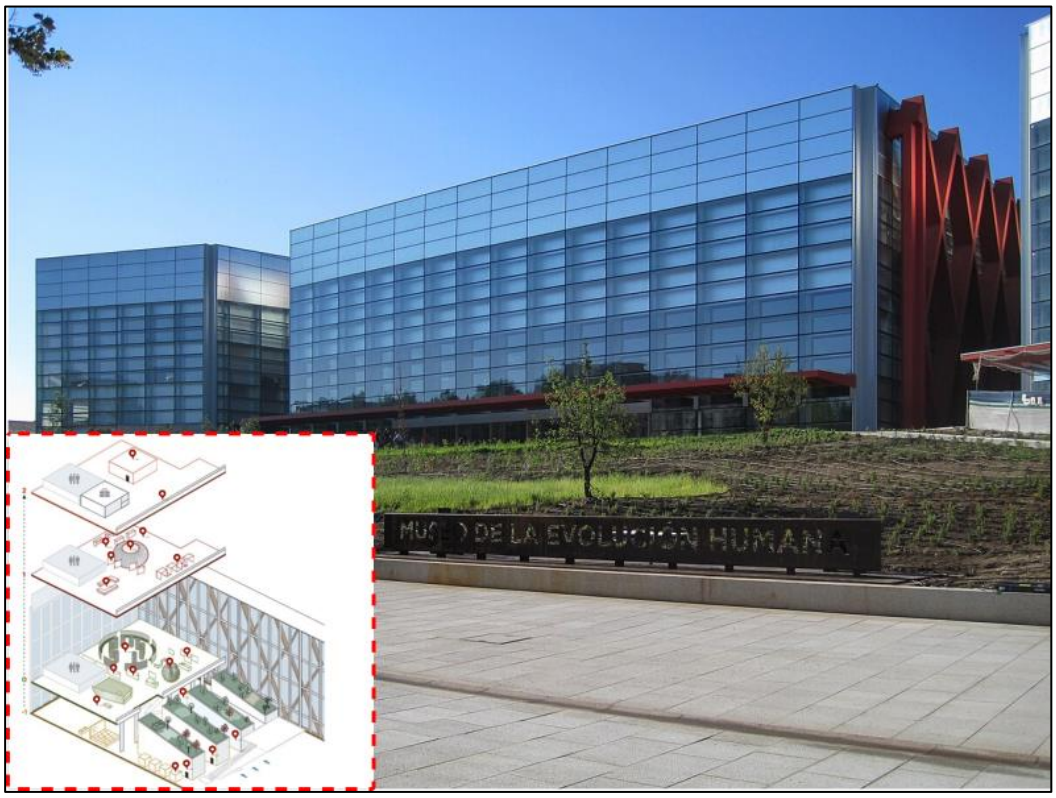

*Figure 15: Pictures of the Museo de la Evolución Humana, **down left** is the distribution of the space in the building ©Wikipedia*

Between 2002 and 2003, the excavations of sepulchral material took place in 3 areas : The Cloister, The Church and the Chapter room. Then in 2004 they expand the project to underneath the cloister basement and in the extreme septentrional area of the nave of the Gospel. Those

three years of archaeological records and documentation have provided a consequent number of 428 skeletons and an indetermined number of ossuary (Figure 16). Inside the cloister individuals are dated form XIV to XVI century and were both adults and children associated with bronze smalls pins and sometimes a piece of money inside the hand. Then in all the area of the church and the chapter room, compartmented and superposed tombs and graves with both inhumations and ossuary were excavated from the XVI to the XIX century.

This funerary material provides important information on the quality of life at this different period of time and on funerary cultural behaviours of the population. Indeed, it is clear that

Figure 16: ***Left*** *excavation of an ossuary,* ***right*** *excavation of a burial ©J.A Casilla Garcia & Gema Adan Alvarez (2005)*

certain areas were dedicated to inhumated people from a low societal position like farmers and merchants mostly in ossuary grave in contrast with the inside of the church for example where it has been found individual inhumated alone. Alongside positional discrimination, examining post-cranial bone traces reveals a significant prevalence of diseases such as syphilis and tuberculosis. Analysing the tooth growth patterns in children also allows archaeologists to identify signs of malnutrition.

Those years of excavation resulted in a consequent well contextualised skeleton collection, allowing to perform numerous varied paleoanthropological and ethnographical analyses. In 2016, 50 individuals have been chosen regarding the well conservation of their hand bones and

have been in the focus of researcher observations. Their phalangeal and metacarpal morphology, as well as their enthesis dimensions, have been studied and published (Bucchi et al., 2022; Karakostis & Lorenzo, 2016).

3.2.NUMBER OF INDIVIDUALS

In this master thesis, we will focus on part of the San Pablo collection, which includes the carpal bones of 40 individuals (20 women and 20 men) with both complete and incomplete wrist skeletons (i.e., 453 bones). During the process of collecting virtual images, each sample was simultaneously referenced with various comments regarding the status of the bones (e.g., half/partially broken, missing, altered, mirrored) (Table 3).

The bone collection for scanning was organized in plastic bags, for each individual containing both the left and right hands skeleton, divided into distinct lots. Additionally, within these larger bags, smaller ones were used to separate the proximal, middle, and distal phalanges from the metacarpals and carpals. Each bag was labelled as follows: **SP-** (for San Pablo) **02 or 03 or 04-** (for the year of excavation) **– X** (individual number) **– Right/Left – XXX** (bone identification). The bones that were unaltered and complete were named "**well preserved**".

Although a template of landmarks for the pisiform is proposed, including them in the sample for the modularity test was reducing the number of complete wrist (wrist that are composed by the 8 carpals). Additionally, the pisiform was not included in the clinical biomechanical models used for the *a priori* hypothesis created for the test. Consequently, Pisiform were removed from the sample used in modularity study and several figures, tables, and interpretations use the term "full/complete wrist" falsely, as they include only seven carpals instead of eight. Only **hypothesis 1bis** proposes running modularity tests with all eight carpals.

Left hand which has the more **well-preserved** bones were chosen to conduct the sexual dimorphism analysis. Only **well-preserved** bones were kept without Pisiform as it was hardly reducing the sample size if it was kept in the sample. Consequently, a total of 201 carpal bones were kept for the sexual dimorphism studied (Table 1)

Table 1: Material for sexual dimorphism analyse number of each carpal from men and women individual

	Women	Men
HAM	12	12
CAP	16	14
SCA	16	18
TRD	15	15
TRM	14	15
TRI	15	12
LUN	13	14

For the modular signal investigations, 23 well-preserved complete wrists (meaning seven carpals only) were retained for analysis (12 right and 11 left), totalling 161 bones (Table 2). 12 left and 12 right **well-preserved** bones were mirrored in order to amplify the sample allowing to complete the sample with seven right and nine left wrists (Table 2). Thus, 39 wrists (19 right and 20 left) were used for the modularity test, representing a total of 273 bones, including 24 mirrored bones and 249 original bones. Sixteen left and right wrists had at least one carpal mirrored, and 23 left and right wrists were complete without mirroring needed. In total, 18 individuals had both their right and left wrists analysed, two individuals only their left wrists, and one only their right wrist (Table 2). Among the 21 individuals, three were missing carpals in both left and right wrists, while four were missing carpals only in their right wrist and six only in their left wrist.

For clarification, <*> indicates that mirrored bones are included in the sample. The effect of adding mirrored bones to the sample is also statistically investigated further (see Table 6).

*Table 2: quantity description of bones in each samples wrist and wrist**

well preserved wrist* description				
	number of wrist *	total of bones	mirrored bones	number origines bones
RIGHT	19	133	12	121
LEFT	20	140	12	128
TT	39	273	24	249

well preserved wrist description		
	number of wrist	total of bones
RIGHT	12	84
LEFT	11	77
TT	23	161

Table 3: Total of bones regarding their status (mirrored, well preserved, altered/broken) ; (*) are samples including mirrored bones.

Totaux without mirrored bones			
	all bones (complete, broken, altered)	complete well preserved bones	altered broken bones
Right bones	**217**	**198**	**19**
eft bones	**236**	**223**	**13**
TT	**453**	**421**	**32**

Totaux with mirrored bones			
	all bones (complete, broken, altered, mirrored)	complete well preserved bones	mirrored
Right bones *	**228**	**210**	**12**
Left bones *	**249**	**235**	**12**
TT	**477**	**445**	**24**

3.3. WRIST BONES DESCRIPTION

Pictures of the best preserved wrist of the sample were token in order to demonstrate the correct siding between dorsal and palmar view of each bones, as well as their anatomical placement within the wrist (Figure 18; Figure 19). They are known for being difficulty to visualize in 2D and even in 3D. It comes from both the irregular shape on each of carpal's numerous facet, and their tendency to be very closed and connected to each others as a very small and highly compacted anatomical units (Figure 17).

Additionally, Figure 20 presents an image of an unusual case of arthritis in a male individual localized solely on the trapezium bones of both hands. This figure is included in the thesis due to its exceptional development, which gives the bones a very distinct shape. The bilateral manifestation of this condition further highlights its rarity and leads to the hypothesis that the arthritis may result more from repetitive mechanical movements than from trauma. Arthritis is

a pathology that can be observed in fossil bones by the presence of polished surfaces caused by eburnation, along with significant bone growth and highly modified joint surfaces.

Figure 17: Picture of a complete right hand in palmar view ©Charline FORAY

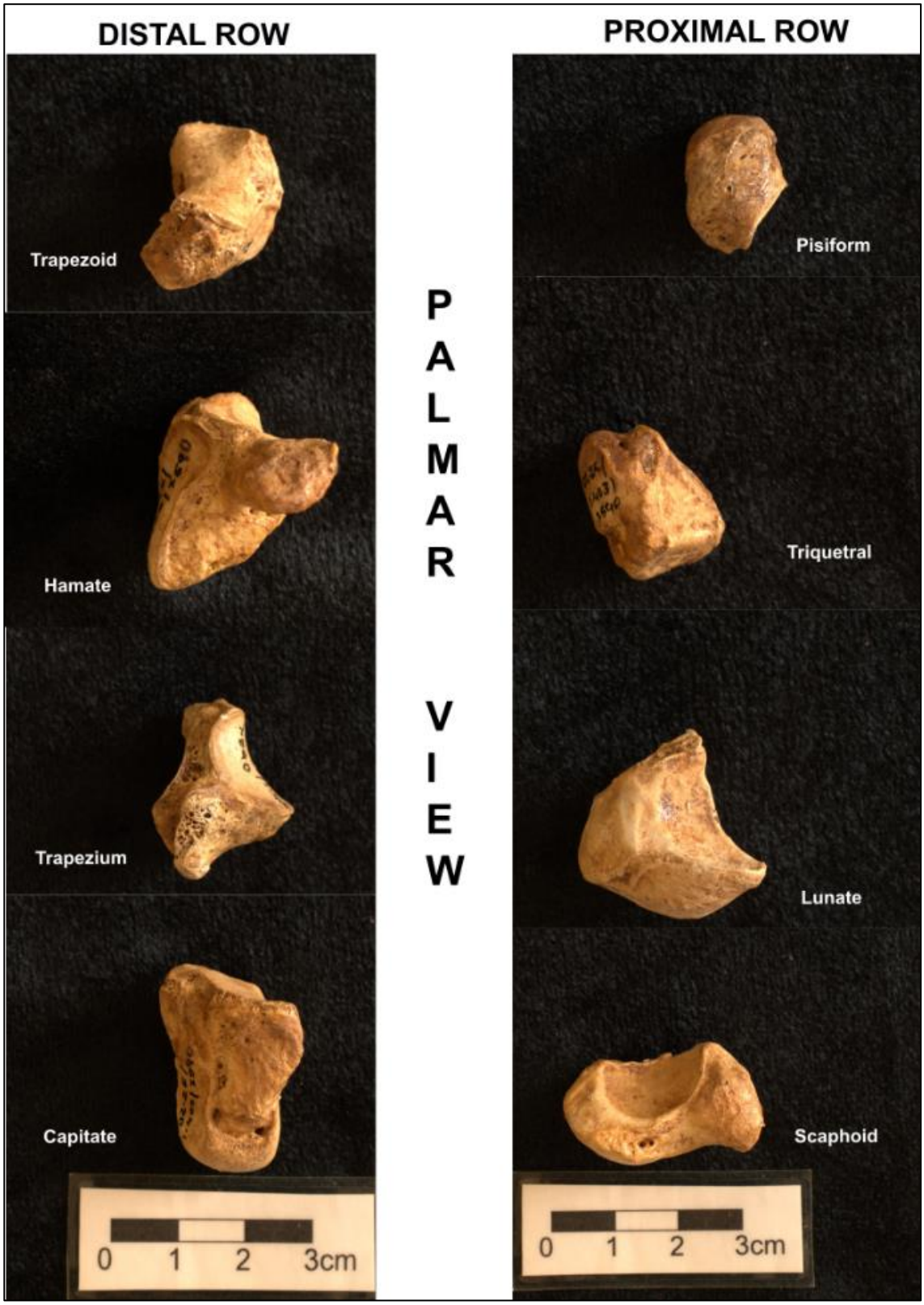

Figure 18: all the carpal bones in palmar view ©Charline FORAY

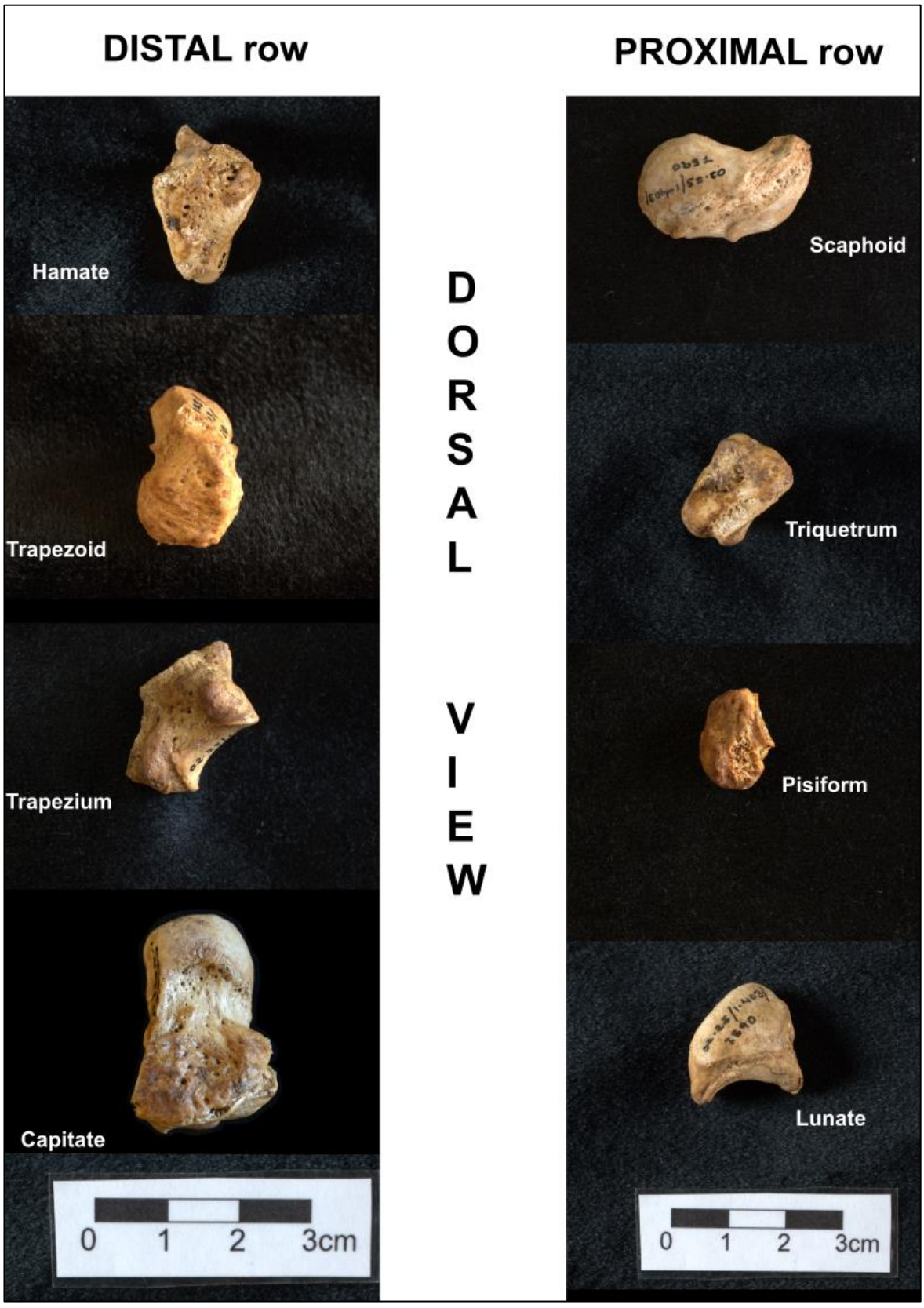

Figure 19: all the carpal bones in dorsal view ©Charline FORAY

Figure 20: Left hand missing the pisiform of individual 88 that had arthritis on trapezium left and right as well. Around the hand are the pictures of trapezium left in lateral, medial, dorsal and palmar view ©Charline foray

4. METHODOLOGY

The carpals from the San Pablo collection were all scanned using the same 3D scanned advanced tool. The geometric morphometric protocol for landmark configuration and Procrustes fitting was consistently applied across both the sexual dimorphism and modularity studies. However, not the same Procrustes fitting values generated by the GEOMORPH package in R are used, reflecting the distinct analytical focus of each study.

4.1.ACQUISITION OF 3D MODELS

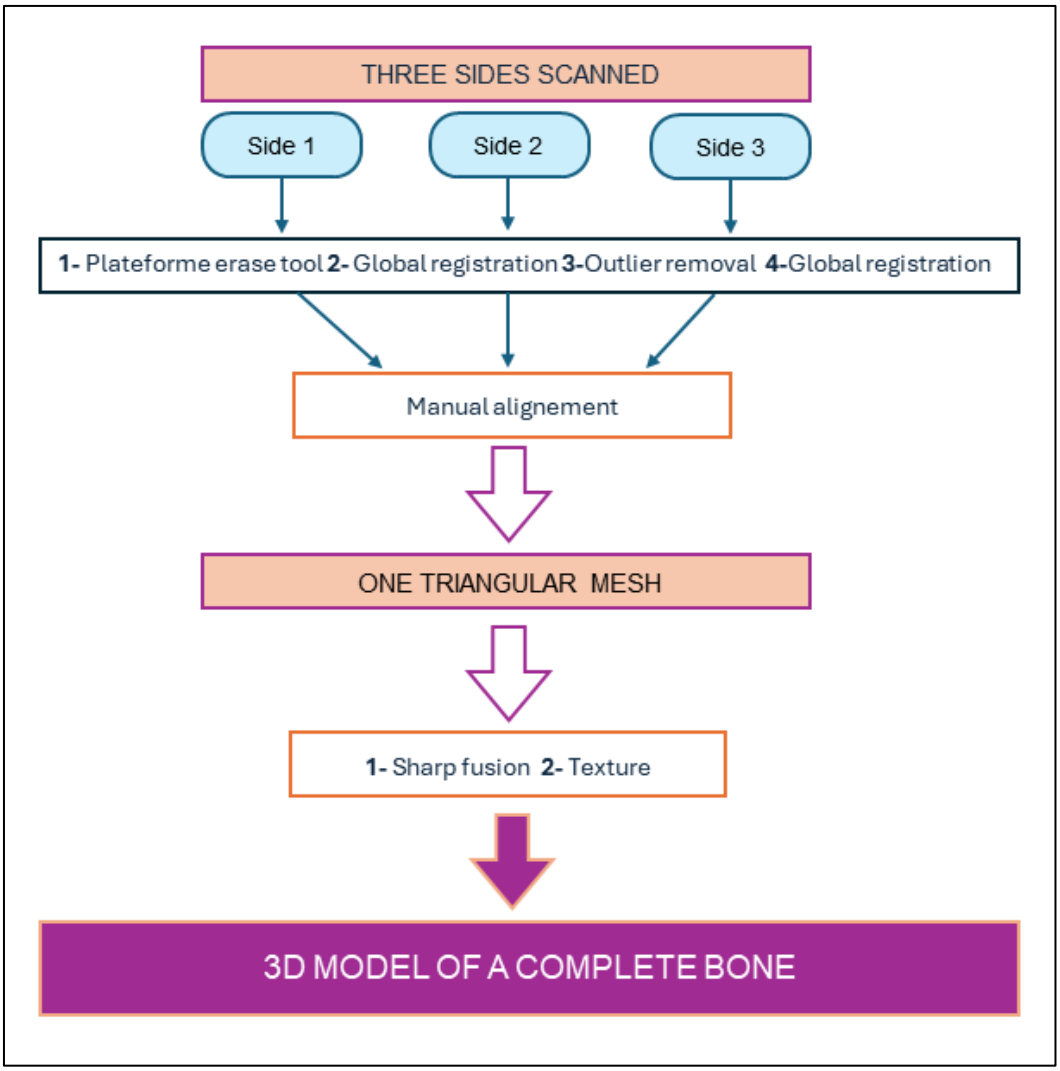

Figure 21: illustration of the established scanning protocol resulting into a 3D complete mesh of the bone

All bones were obtained with the 3D scanner Artec Spider. It is a high-resolution 3D scanner based on blue light technology with an accuracy up to 0.05mm and a resolution up to 0.01. Thanks to a technology of reflective light with both projector and captors it creates high resolution triangular mesh and polygonal 3D model with or without texture. A triangular mesh is a collection of point joined together which form triangles and interpolates to acquiring a surface. It wise to note that for these interpolating surfaces the denser is the distribution of sampled points the best will be the representation of the bones surface. On average, and by taking in account the time availability and storage capacity, the 3D models for this master thesis were made with triangular meshes of 600 frames (Figure 22). Due to the limited information resulting from the relative positions of the bones on the rotating platform, we initially scanned at least three different sides of the bones to ensure we captured the complete shape (Figure 21).

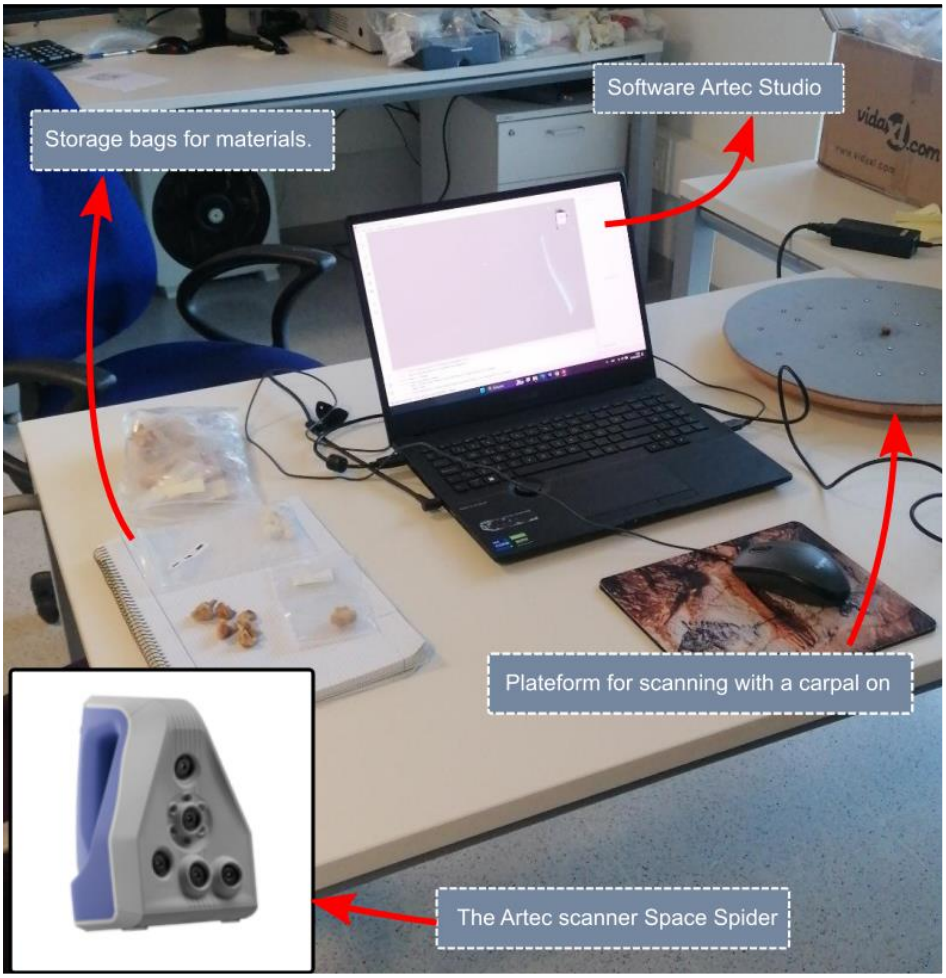

Figure 22: the paleoanthropological office with the raw material, the Artec spider scan and the laptop that include the Artec software

Subsequently, the cleaning, manual alignment, and fusion of each scanned surface of the bone were performed using Artec Studio Software 2016©. This software provides specific tools at each step, facilitating the workflow. The bones were placed on a rotating platform, and the

points cloud generated by this one was removed from the mesh using the platform erase tool. The global registration algorithm aligned all frames surfaces to create a single coordinated system. This process, combined with the outlier removal tool, ensured a frame registration quality (referred to as "Spider Error" in Artec Studio) with an acceptable error range of 0.1-0.2. However, due to the complex and irregular shapes of the carpal bones, automatic alignment was unsuccessful, and the assembly of the three scans into a single unit was done manually. This resulted in a triangular mesh that underwent sharp fusion to produce the final polygonal 3D model. Sharp fusion is the most precise fusion mode available in Artec Studio and was applied with a resolution of 0.1mm, the highest provided by the software. Finally, a texture was applied to the polygonal 3D model.

4.1.1. Bones siding

A review of the correct siding (Table 4) for each bones was conducted on the 3D models with the siding technique delivered in White's book *Human osteology* that I resume in the following table (White et al., 2012).

Table 4: siding methods for each carpal, modified from White et al (2012)

PISIFORM	With the articular facet towards you, orient the bulk of the non articular surface up. The groove and the bulk are displayed towards the side from which the bone comes from.
TRIQUETRAL	Hold the pisiform facet up with the edge between the hamate and lunate oriented vertically. The hamate facet is on the side from where the bone comes.
LUNATE	Place the bone with the concave facet for the capitate in front of view with the triquetrum facet up. It points towards the side from which the bone comes.
SCAPHOID	Place the capitate facing the ground with the tubercule pointing up. It is on the side from which the bone comes.
TRAPEZIUM	Place the bone on a flat surface with the ridge on top and away from you. The scaphoid and trapezoid facet are on the side from which the bone comes from
TRAPEZOID	Place the biggest non articular facet on the ground with the V-shape edge facing you. The "toe part" is pointing the side from which the bone comes from.
CAPITATE	Place the head point up with the facet for the hamate facing you. It is on the side from which the bone comes.
HAMATE	Place the biggest non articular facet on the ground with the metacarpal facet in front of you. The hook is on the side from which the bone comes.

4.1.2. Bones mirroring

When one or two carpals were missing to complete a wrist, they were mirrored if the counterparts from the other side of the same individual were available and well preserved. They were made with the "mirror" tools in 3Dslicer. Seven right and nine left wrists were completed this way. Later, univariate statistics were conducted in order to check for a significative difference between modularity results from sample with only originals bones and sample with originals and mirrored bones.

4.2.GEOMETRIC MORPHOMETRY METHODS

Morphometrics, or morphometry, implies the study of variability in the form (shape and size) of organisms and objects. Most applications employ 2D or 3D landmarks to measure and analyse shape and size. Here, we propose a two-step protocol with a 3D landmark template, based on commonly used protocols in morphometric studies (Adams, 2016; Bookstein, 1991; Corruccini, 1987; Hammer & Harper, 2006; Jungers et al., 1995; Klingenberg, 2009).

4.2.1. Landmark configuration

Due to shape irregularities, 3D anatomical landmarks were best to investigate shape. We decided to reuse the five landmarks Bucchi used on the capitate, trapezium, lunate, and scaphoid (Bucchi et al., 2022), and added five new landmarks to them taking into consideration articulation and morphology. For the trapezoid, hamate, and triquetral, each of their landmark template is a mix of previously published and approved landmark positions, as well as newly proposed ones based on anatomical and biomechanical understanding and a bibliographic survey of landmark positions. This survey revealed a lack of methodological protocols for proposing landmarks on carpal bones (A. Peña, 2018; Bardo et al., 2023; C. M. Orr et al., 2010).

Focusing solely on Homo sapiens wrist bones allowed us to expand upon Ana Bucchi's work on modularity. Including other hominin families (such as Gorilla and Pan) in our sample would have increased the likelihood of not finding enough individuals with all eight carpal bones. As a result, this master's thesis gathered a template of 10 landmarks type I and II identified as homologous on all carpal bones of the sample (pisiform, lunate, triquetral, scaphoid, trapezium, trapezoid, capitate, hamate) (Figure 33 ; Figure 34). All landmarks were manually placed on

the surface meshes in ©3D Slicer. During a day, the types of carpals on which the set of landmarks were placed was randomized. Indeed, by working continuously on only one types of carpal, then changing to another one can led to systematic error because of skill improving through time. Or on the contrary error from awareness (Hammer & Harper, 2006).

In order to assess the none intra-observer error, the set of anatomical landmarks were placed six times on one of every type of carpals (Bardo et al., 2023) (Figure 33 ; Figure 34) and repeatability was assessed by statistical test. Several days were separating the task on the same bones and set of landmarks on different types of carpals were placed in the same day. GPA produced Procrustes coordinates for all repeat specimen, and ANOVA test were conducted on R**.** Below is a list with the description of the ten landmarks created for each carpal with their localization on a 3D mesh with texture.

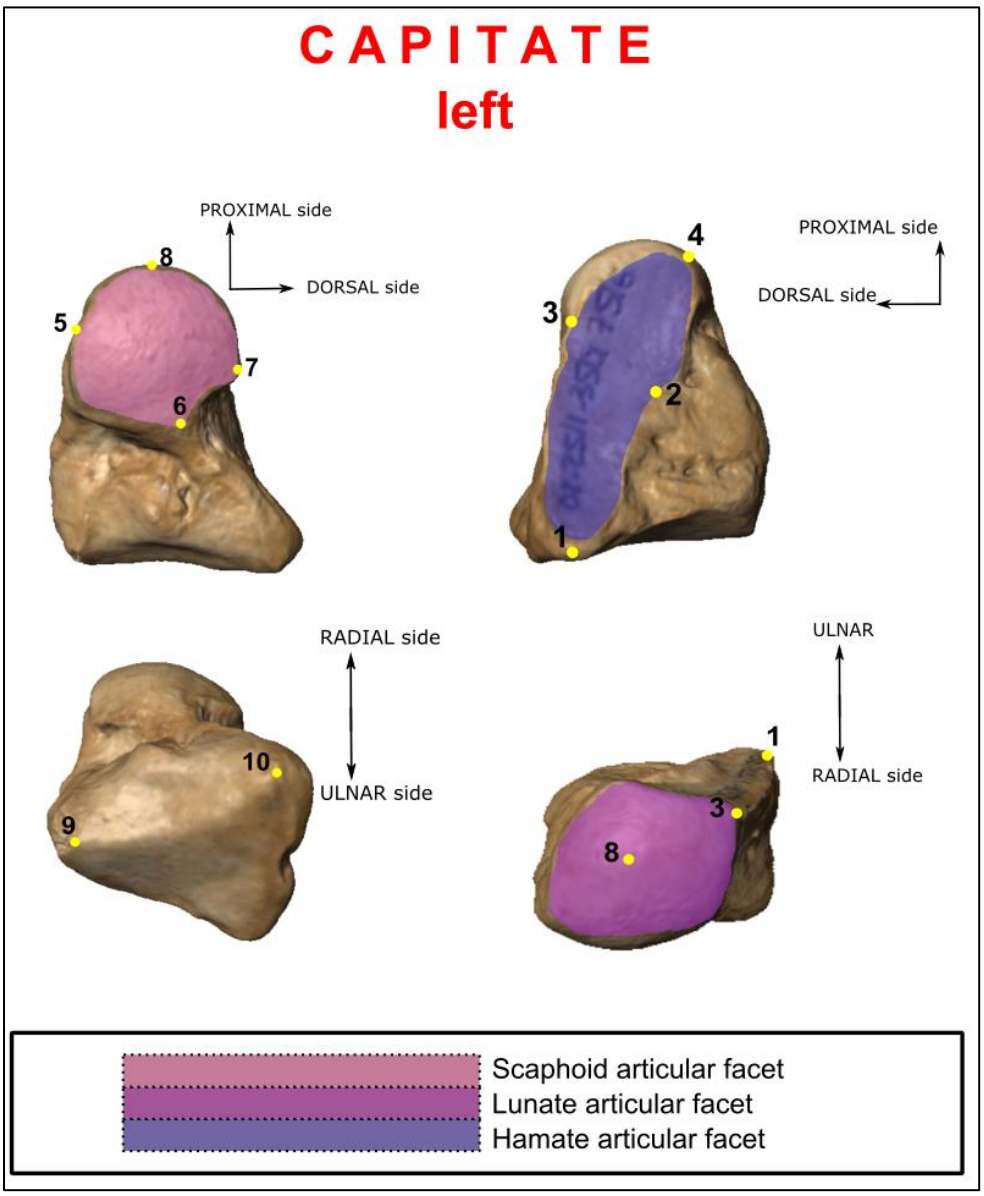

CAPITATE	
1	Junction most postero-medial between the facet of hamate and Metacarpal 3
2	Most palmar point of the hamate facet
3	Anterio-proximal junction between facet of hamate and lunate
4	Palmar point of hamate facet
5	Palmar point of scaphoid facet
6	Distal point of scaphoid facet
7	Anterior point of scaphoid facet
8	Proximal point of scaphoid facet
9	Palmar junction between Metacarpal 2 and 3
10	Anterior junction between Metacarpal 2 and 3

Figure 23 : landmark template for the capitate

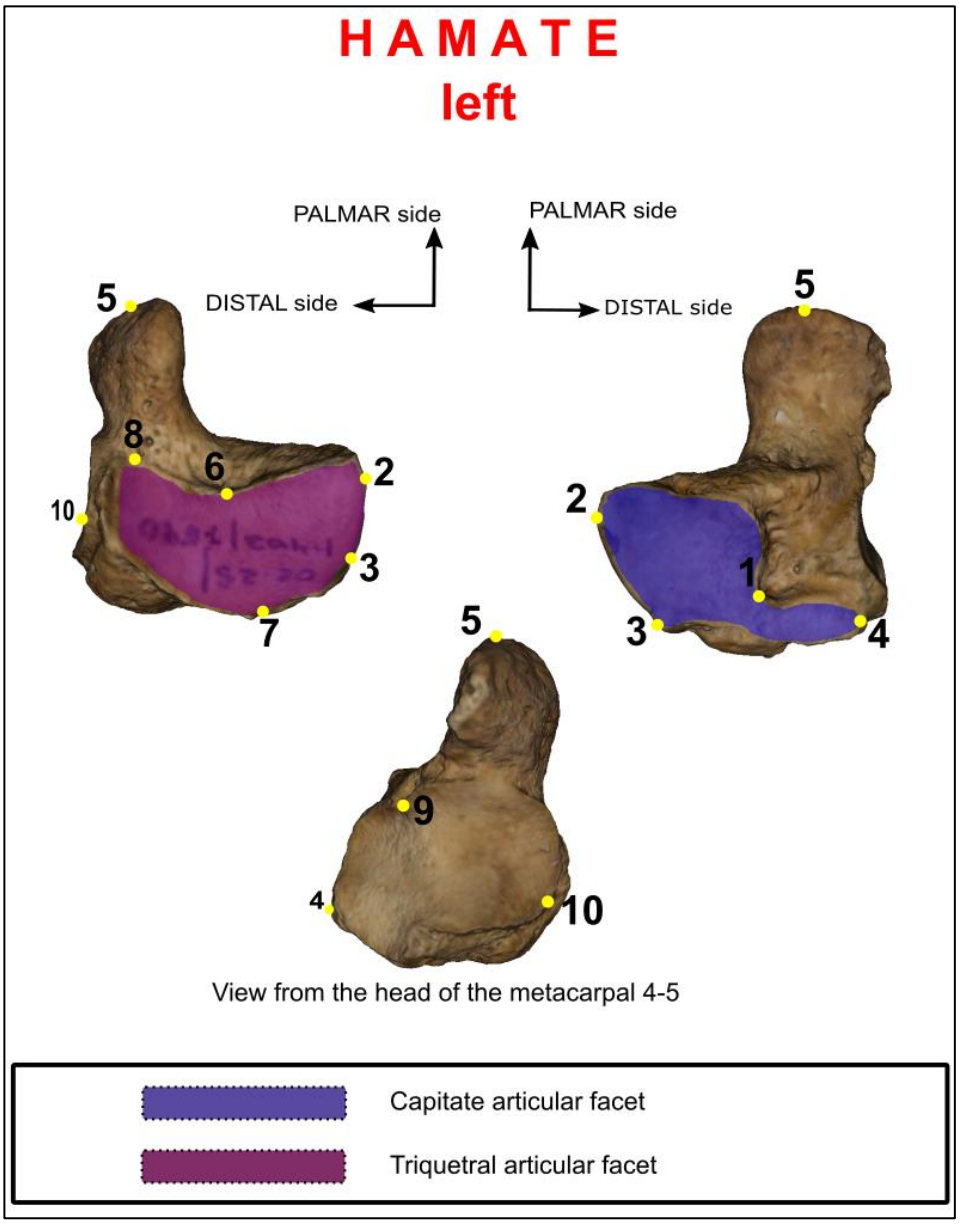

HAMATE	
1	Point of maximum inflexion on the palmar border of capitate surface
2	Most proximal point on the junction of triquetral and capitate surfaces
3	Junction of the triquetral and capitate surfaces on the dorsal side
4	Most distal point of capitate surfaces
5	Most distally protruding point of the hamulus
6	On the triquetral surface, point of maximum inflexion on the palmar side
7	On the triquetral surface, most convex point of the dorsal side
8	On the triquetral surface, distopalmar border
9	Junction of metacarpal 4 and 5 on the palmar side
10	Ulnodorsal border on the metacarpal 5 surface

Figure 24: Landmark template for the hamate

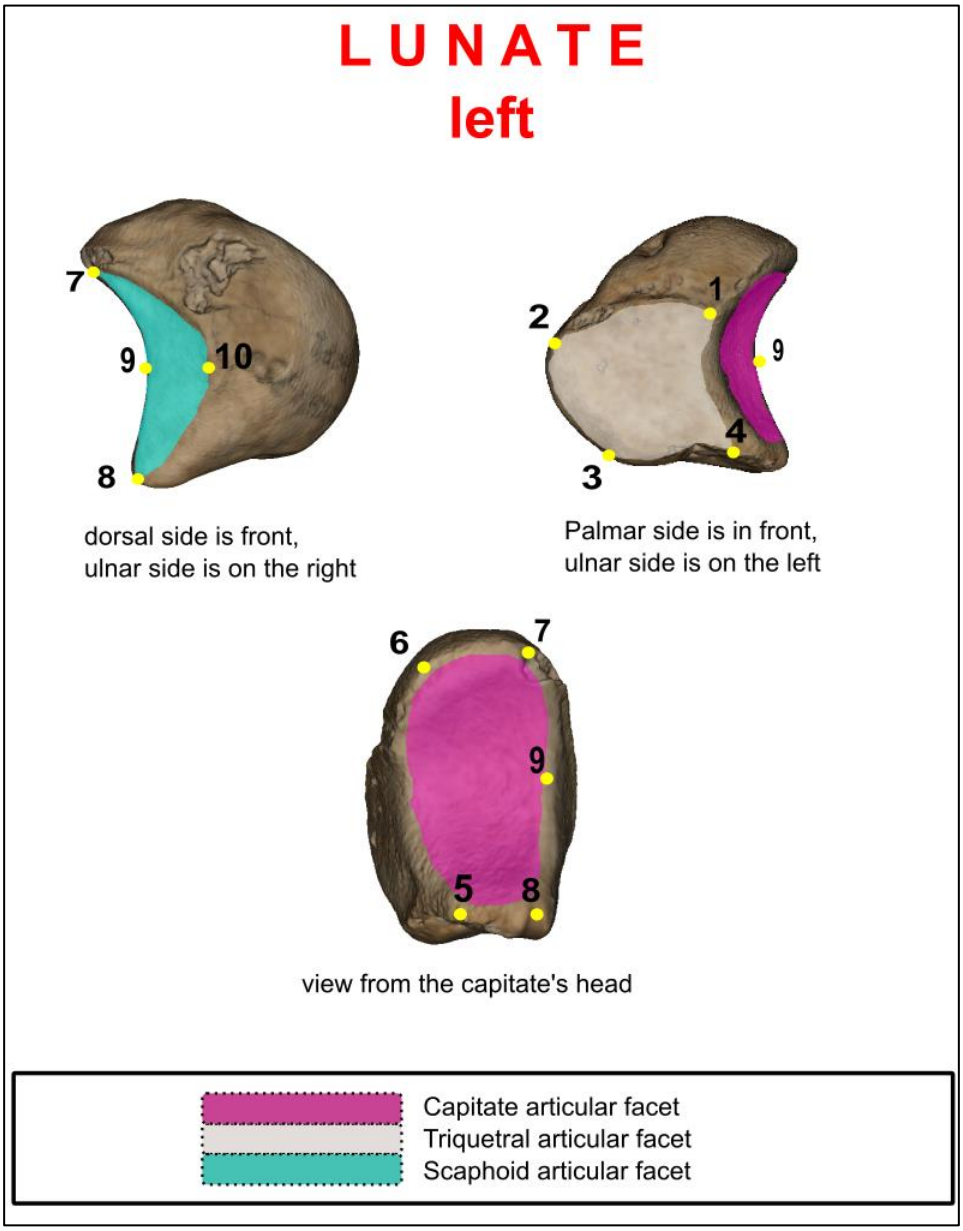

LUNATE	
1	Most radio-proximal point of the triquetral facet
2	Most ulno-proximal point of the triquetral facet
3	Most ulno-distal point of the triquetral facet
4	Most radio-distal point of the triquetral facet
5	Palmodistal point of the capitate
6	Palmoproximal point of the capitate
7	Dorsoproxiaml point of the junction between capitate and scaphoid facet
8	Dorsodistal point of the junction between capitate and scaphoid facet
9	Point of most inflexion of the capitate and scaphoid junction
10	Point of most ulnar inflexion of the scaphoid facet

Figure 25: Landmark template for the lunate

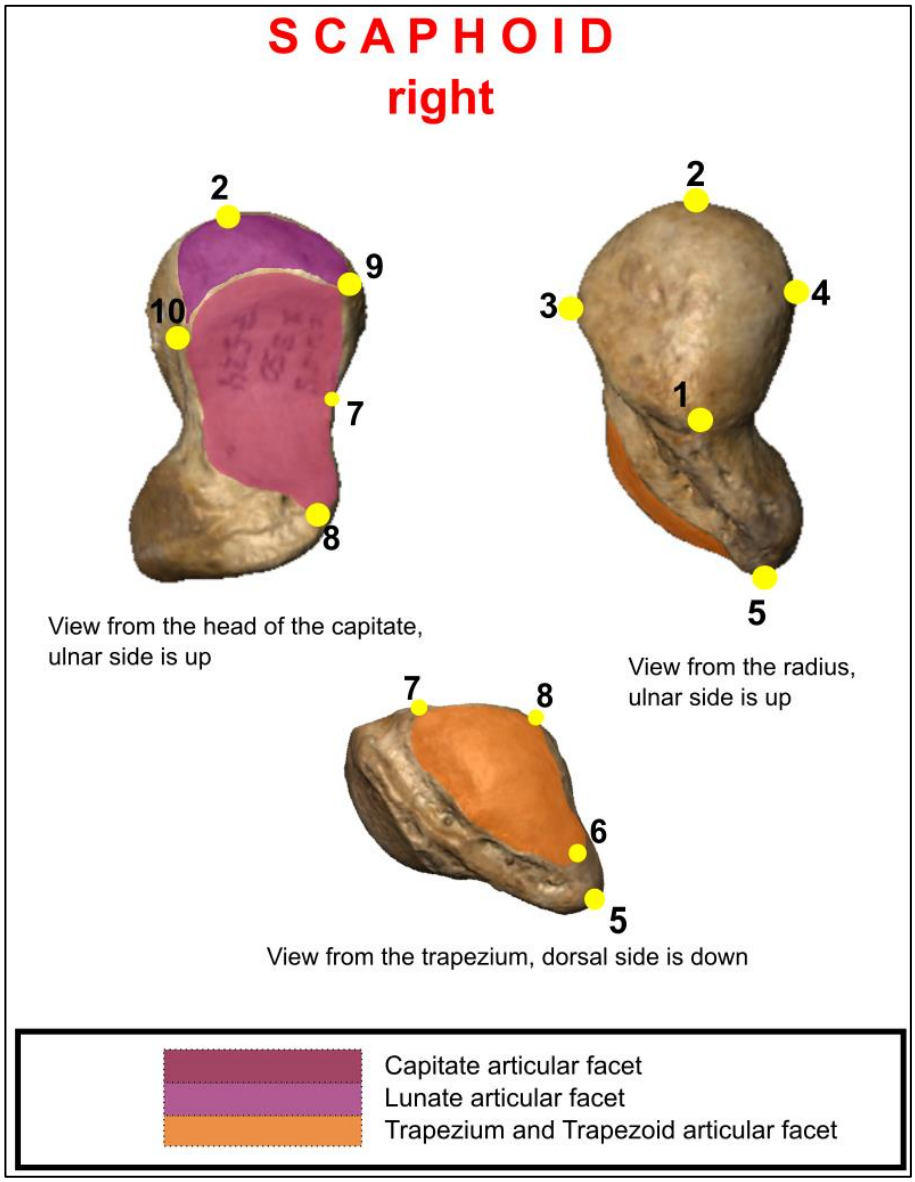

SCAPHOID		
	1	Most radial point of the radius facet
	2	Most ulnar junction point between radius and lunate facet
3		Most dorsal point of radius facet
	4	Most palmar point of radius facet
	5	Highest point of the scaphoid tubercule
	6	Most radial point of the trapezium facet
	7	Most inflexion point on the junction of trapezoid and capitate facet
	8	Most dorso-radial point on the junction of trapezium and capitate facet
	9	Most dorsal junction between capitate and lunate facet
	10	Most palmar junction point between capitate and lunate facet

Figure 26: Landmark template for the scaphoid

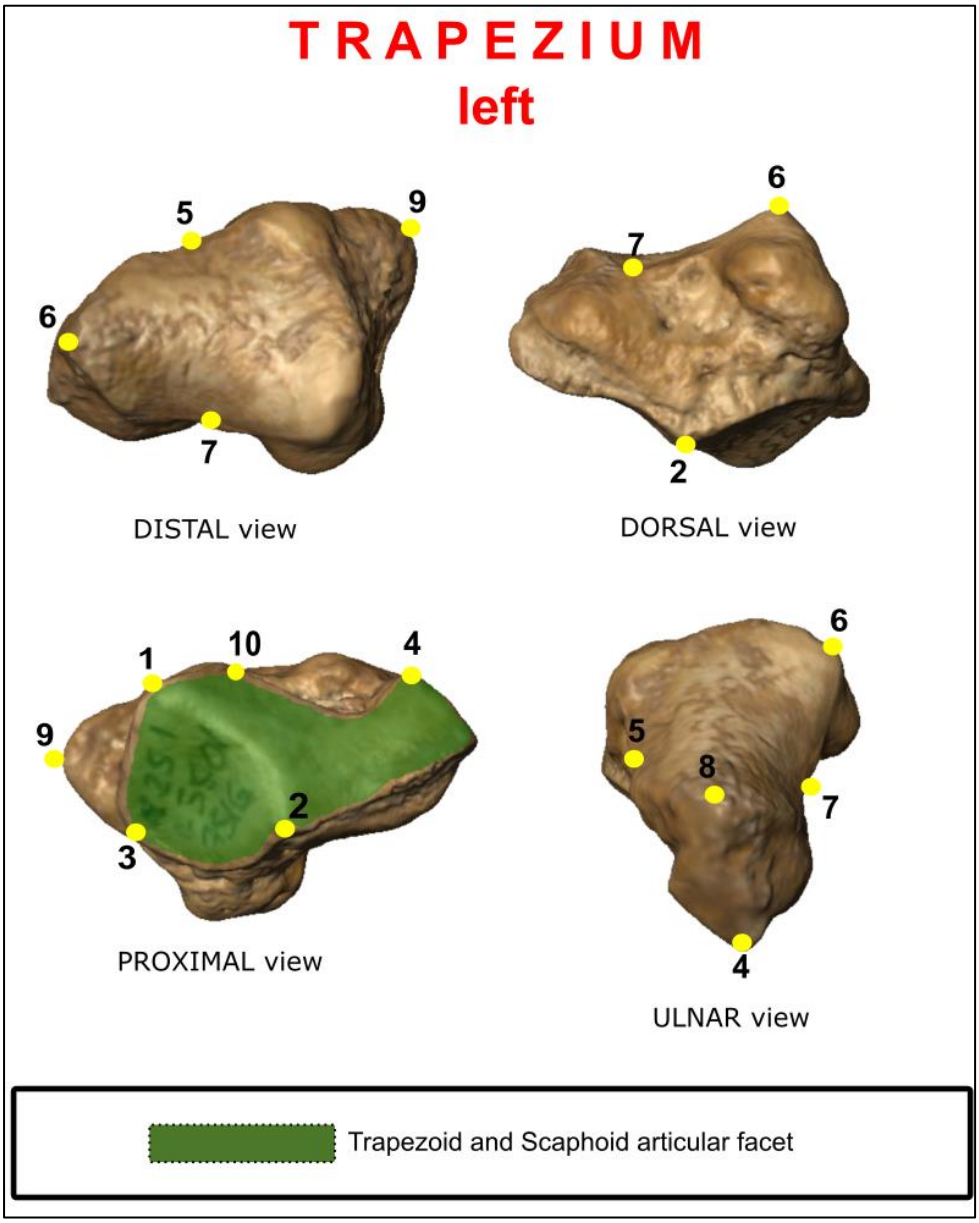

TRAPEZIUM	
1	The most anterior point of the scaphoid articular surface
2	Most posterior point of the scaphoid articular surface
3	Most distal point of the scaphoid articular surface
4	Most distal point of the metacarpal 2 articular surface
5	Most palmar point of the distal articular surface
6	Most radial point of the distal articular surface
7	Most dorsal point of the distal articular surface
8	Most ulnar point of the distal articular facet
9	Point of maximum curvature of the tip of the tubercule of the trapezium
10	Point on scaphoid facet at the minimum distance with point 5

Figure 27: Landmark template for the trapezium

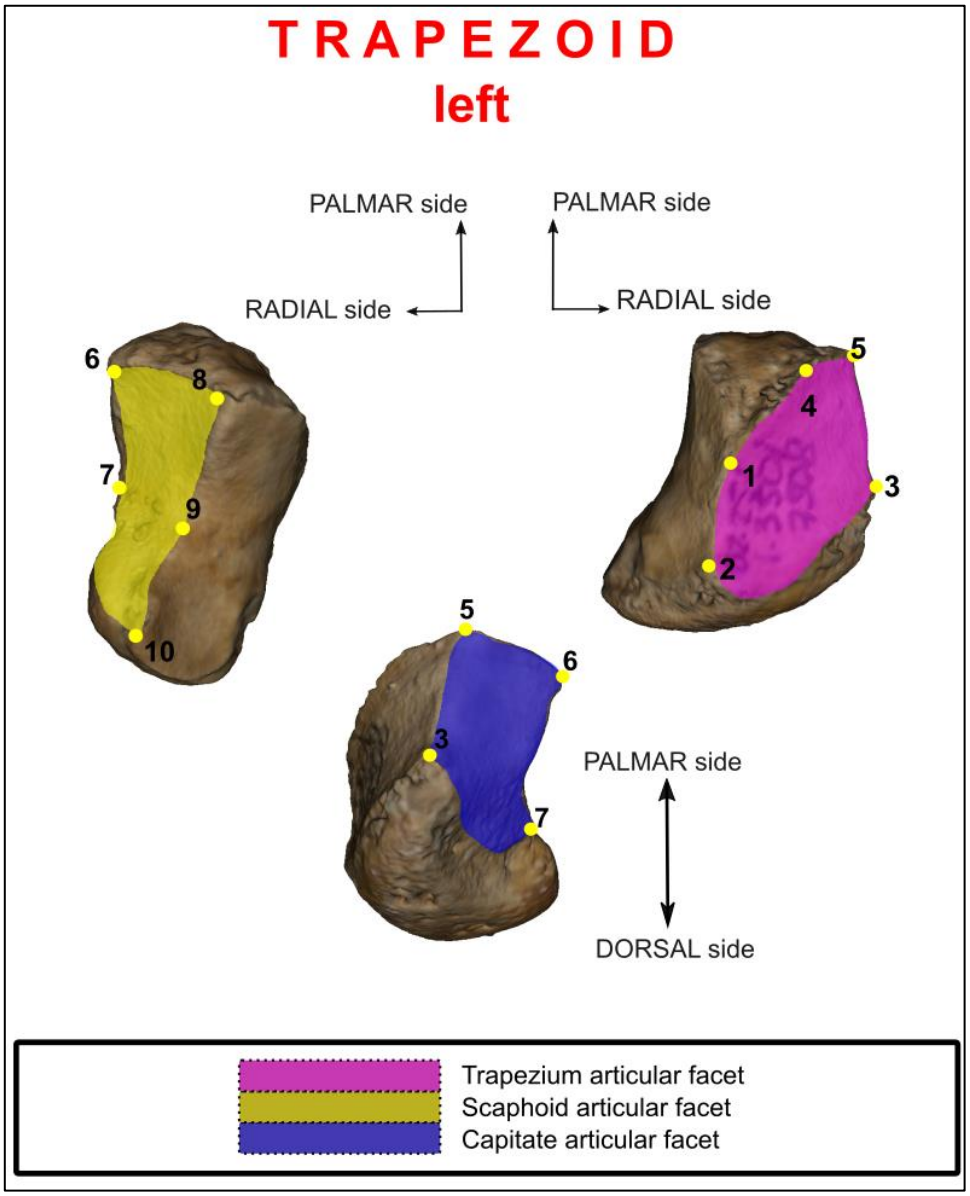

TRAPEZOID	
1	Most palmar point on the junction between trapezium and metacarpal 2 facets
2	Most dorsal point on the junction between trapezium and metacarpal 2 facets
3	Most dorsal point on the junction between trapezium and capitate facets
4	Point of maximum palmar inflexion on the trapezium facet
5	Most palmar point on the junction between trapezium and capitate facets
6	Most palmar on the junction between scaphoid and capitate facets
7	Most inflexion on the radial side of the scaphoid facet
8	Most palmar point on the junction between scaphoid and metacarpal 2 facets
9	Most inflexion on the junction between the scaphoid and metacarpal 2 facets
10	Most distalo-dorsal point on the junction between the scaphoid and metacarpal 2 facets

Figure 28: Landmark template for the trapezoid

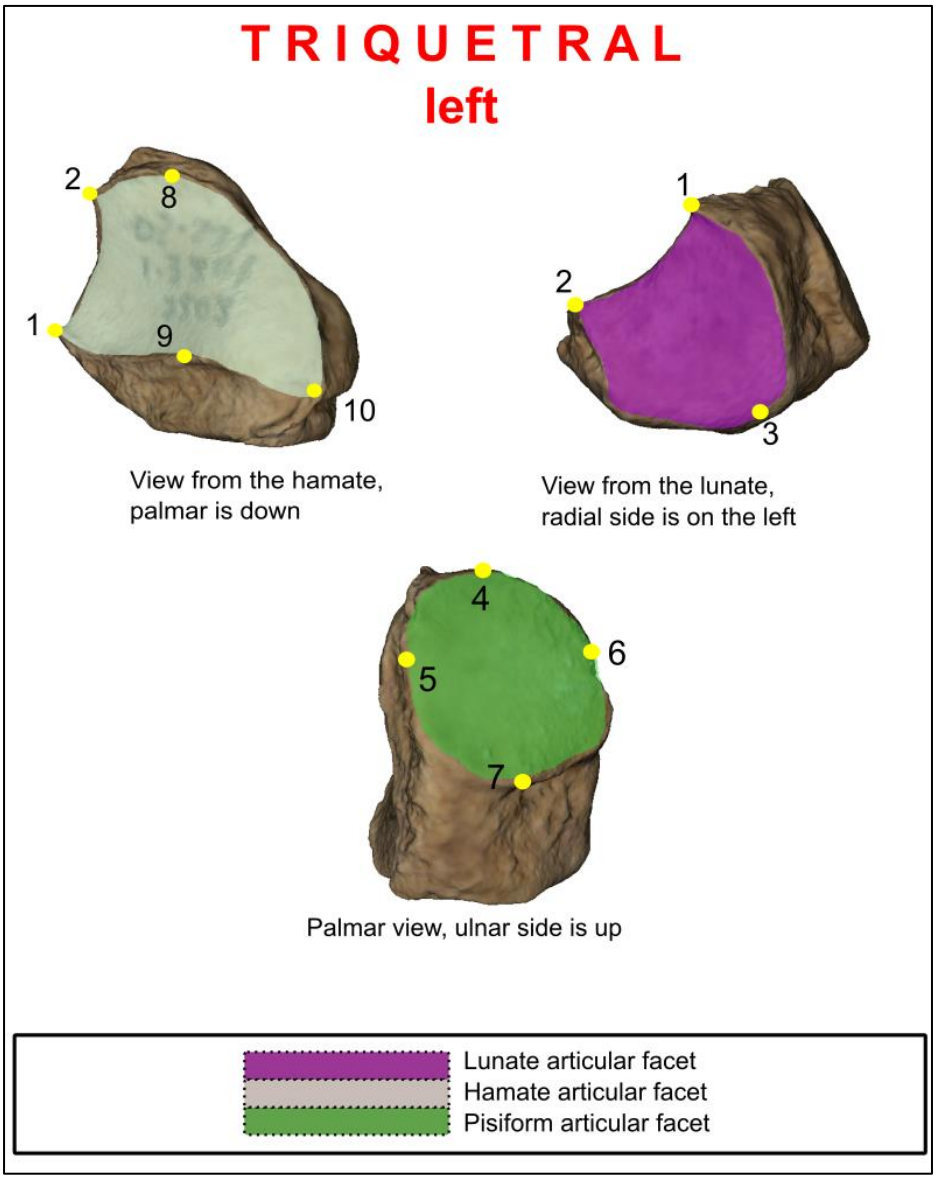

TRIQUETRAL	
1	Junction of the hamate and lunate facet on the palmar side
2	Junction on the hamate and facet on the dorsal side
3	Most palmar point of the lunate facet
4	Most distal point of the pisiform facet
5	Most radial point of the pisiform facet
6	Most ulnar point of the pisiform facet
7	Most proximal point of the pisiform facet
8	Point of most dorsal inflexion on the hamate facet
9	Point of the least palmar inflexion on the hamate facet
10	Most palmar point of the hamate facet

Figure 29: Landmark template for the triquetral

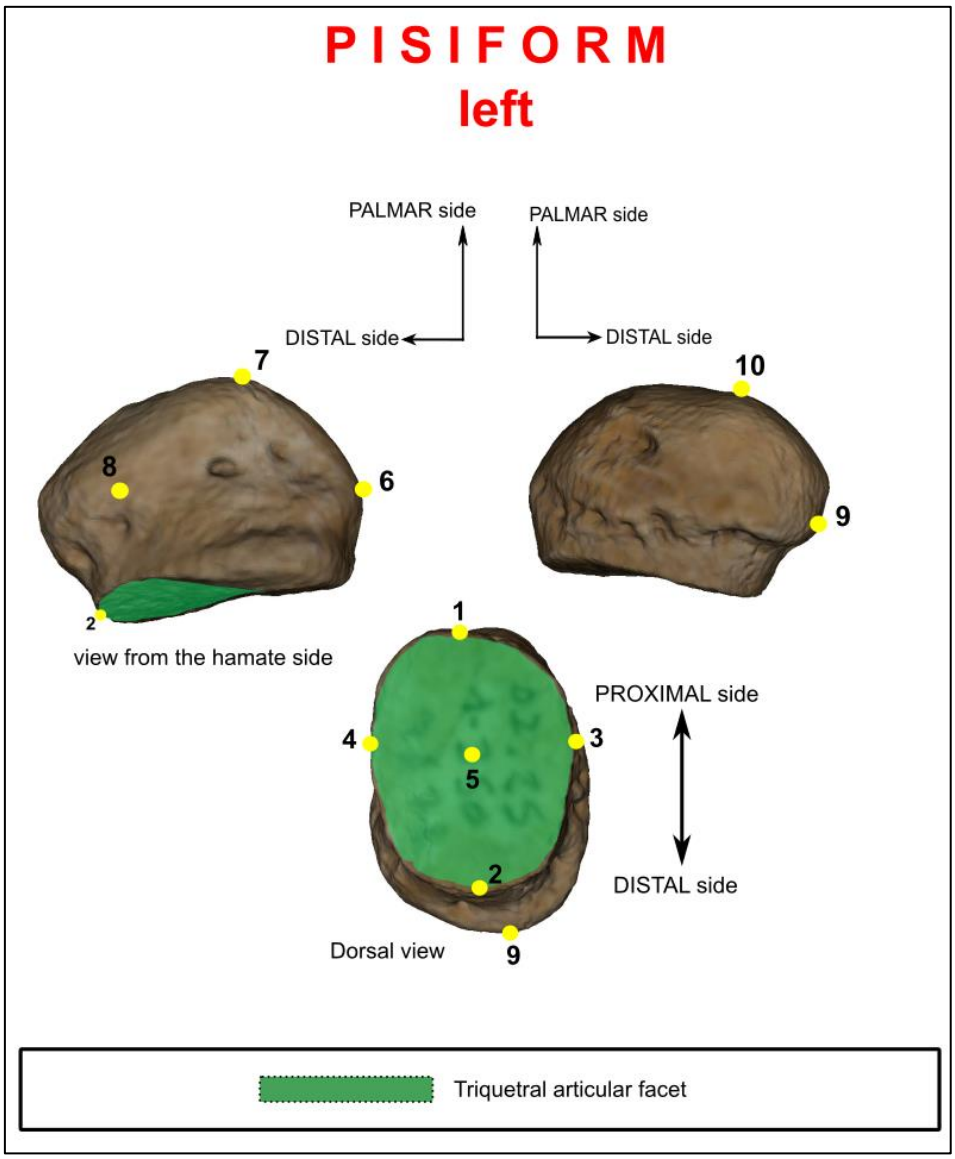

PISIFORM	
1	Most proximal point of the triquetral articular facet
2	Most distal point of the triquetral ovoid facet
3	Most lateral point towards the hamate side of the triquetral articular facet
4	Most ulnar side point of the triquetral articular facet
5	Middle of the ovoid articular facet
6	Proeminent point the bulk below point 1
7	Highest point below point 6
8	Middle of the groove that separates the pisiform's body from the articular facet
9	Most distal point of the distal bulk
10	Highest point of the pisiform body

Figure 30: Landmark template for the pisiform

4.2.2. Procrustes coordinates approaches

- *Sexual dimorphism analysis*

Sexual dimorphism in carpals was investigated by comparing centroid size of each carpal from men and women individuals. Inside the collection, left carpals are the most preserved and are in highest quantity than right carpals. Pisiforms and mirrored bones were removed from the sample for these analyses. Landmarks coordinates in .csv format were combined in 3D array by bones. Value of centroid size were obtained with the function “gpagen” applied on each 3D array and a vector (“Male”-“Female”) was applied.

- *Integration and modularity*

A study aiming to use Procrustes Shape data for integration and modularity investigations require to decide between two approaches of landmark setting. The work of Andrea Cordini (2019) describes two possibilities defined by morphometricians (Bookstein, Klingerberg, Adams, and others), which are called **within configuration** and **separated blocks**: “*In this case, a morphometrician does a single Procrustes superimposition including all landmarks, obtains a unique set of shape coordinates and then splits these shape coordinates into modules made of different subsets of landmarks* [then, for the separated blocks approach, scholars] *start with the raw data (no superimposition), split them into modules and then perform separate Procrustes superimpositions for each module*” (Cardini, 2019, p. 191). The final decision on the best approach is still under discussion and could significantly influence the results. However, morphometricians have argued that the "within configuration" approach might lead to more interpretable outcomes (Cardini, 2019). In this configuration, relative size and positional differences are preserved throughout the analysis because all data are in a common shape space. It is important to note that morphometricians urge caution in interpreting superimposition Procrustes analysis, as this field still requires further research to avoid spurious results when testing integration and modularity(Cardini, 2019; Klingenberg, 2009, 2014).

Following these recommendations, and in order to respect the **within configuration** methods, each set of landmarks were registered from 3Dslicer in a .csv format, upload in Rstudio software, and stacked into one set including all 3Dlandmarks of the carpals from all individuals (Triquetral, Lunate, Scaphoid, Trapezium, Trapezoid, Capitate, Hamate).

The next steps have been applied separately for right and left carpals : A General Procrustes analysis was made with the function " gpagen" in R, which was applied on the new "3D array stacked". The unique set of *Procrustes shapes coordinates* obtained was split into modules in R, according to each *a priori* hypothesis.

Future work on this collection could include semi-landmarks around the articulation of carpals, resonating with Amelie Bardo's work on morphological integration between the trapezium and metacarpal joint facet (Bardo et al., 2023).

4.3.STATISTICAL TEST

Univariate tests were conducted to investigate significant differences between datasets of different variables or the same datasets from different environments. Carpal's shape represented here by the centroid size value given by the "gpagen" function in R is used in sexual dimorphism investigation. Additionally, modularity within the wrist was examined using multivariate analysis and empirical statistical tests with permutation methods from the GEOMORPH package in R.

4.3.1. Sexual dimorphism

Csize of each bone of men and women individuals were compared with a mann-whitney non-parametric test (Shapiro-Wilk pvalue<0.05) with the function "wilcox.test" in R. The creation of a dataframe gathering <statistic value & Pvalue> allowed to register in an excel table every results for all the seven bones. Not removing pisiform was hardly reducing samples in men and women. It was decided to not use the Pisiform in the sexual dimorphism analyses. The distribution of Csize of each bone from males and females' sample were displayed using a boxplot graphic made in R.

4.3.2. Integration and modularity investigations

- *Modular hypothesis*

In order to assess different signal of modularity pattern, 8 alternatives *a priori* models (called here hypothesis) were proposed with distinct modular structure caused by specific kinematic and biomechanic mechanism (Table 5). Most part of the modular hypothesis are three-modules

model except for the hypothesis 2 and 6 which are two-modules models. Only **hypothesis 1bis** proposes running modularity tests with all eight carpals.

Table 5: all the hypotheses use for the modularity study.

Hypotheses	Modules	Description
H1	TRI-LUN-SCA-TRM-TRD-CAP-HAM	All carpals belong to a different module
H1 bis	PIS-TRI-LUN-SCA-TRM-TRD-CAP-HAM	All carpals belong to a different module
H2	TRILUNSCA - TRMTRDCAPHAM	Distal carpals are separated from the proximal ones. ➔ Row theory
H3	TRIHAM – CAPLUN - SCATRMTRD	The eight carpals are divided into 3 distalo-proximal columns from ulnar to radial order ➔Modified from column theory Navaro 1921
H4	TRI – LUNHAMCAPTRDTRM - SCA	Scaphoid and triquetral belong to there own module and other carpals are regrouped in one. ➔Row column theory
H5	HAMTRI – LUNCAPTRD - TRMSCA	Two rotatory distalo-proximal modules in extreme ulnar and extreme radial direction and one column module in the centre ➔Ring model
H6	LUNTRIHAMCAP - SCATRMTRD	Most radial carpal belong to one module, and distal carpal to another. ➔Ovoid Cshape
H7	SCA-LUNTRI - HAMCAPTRDTRM	Proximal row is divided into two modules, distal row belongs to one module. ➔Screw-vice model
H8	SCALUNTRIHAMCAPTRDTRM	All carpals belong to one module

For testing modular hypothesis, nor the RV coefficient (Klingenberg, 2009) , or the Partial Least Squared approach(Bookstein, 1991) were used here. Indeed they are highly affected by the sample size and the number of variables(Adams, 2016). Instead, modular signal in the wrist was evaluated by applying the covariance ratio approach and statistically compared with the effect size measure derived from it (Adams, 2016; Adams & Collyer, 2019). The function " modularity.test" and "compare.cr" in GEOMORPH package in R were used.

- *Covariance ratio (cr)*

The covariance ratio CR proposed by Adams and his colleagues ranges from 0 to positive values. Unlike the Partial Least Squares methods, it can be applied on more than two blocks of Procrustes data by averaging pairwise of CR. It is less sensitive to sample size as well(Adams, 2016). CR ratio lower than 1 indicates high covariance within modules than between (Bucchi et al., 2022; Cardini, 2019). It is assessed via permutations. The algorithm assigned randomly landmarks to different modules and calculates the CR coefficient at each repetition. Finally the original CR is compared with the CR distribution(Adams, 2016).

- *Effect size measures (Zcr and Zpairwise)*

Quantitative methods for statistically comparing the strength of modular signal across datasets were hardly poor in evolutionary biology and morphometry studies in general. The statistical approach MINT (by Marquez 2008) and EMMLi (Goswami and Finarelli 2016) have been showed to have limited performance results (Adams & Collyer, 2019). On the contrary, Adams method (2019) display high statistical power and an acceptable type I error rates. Its approach is doing two tasks : measuring a modular signal "strength" (**the modular effect size Zcr**) of each module hypothesis across a dataset, and execute a two-sampled test to compare pairs of Zcr ($\mathbf{Z_{pairwise}}$ **model of comparison**). Zcr is calculated from the Covariance ratio value and is a standardized test that ensure statistically compatibility with CR whether the number of modules between hypothesis are different or no. In the equation of Zcr, when modular signal is strong, CRobs will be less than $\hat{\mu}_r$ (the expected value of CR under the null hypothesis of no modularity). Thus, more negative the value of Zcr is, stronger is the modular signal.

$$z_{CR} = \frac{CR_{obS} - \hat{\mu}_r}{\hat{\sigma}_r}$$

Then, a pairwise model comparison (using this effect size measures is useful for analytical development and modular signal characterization.

Adams and his colleagues have implemented their methods in the GEOMORPH package in R, and create the function "compare.cr" that is logically using the value <CR> and <effect size Z> of the function "modularity.test". Both of them have been used in the analysis of the dataset for this master thesis.

- *Investigation on the effect of presence of mirrored bones on modularity tests*

The values of Covariance and Zcr of the four datasets (left, left*, right right*) are not normally distributed (Shapiro-wilk pvalue<0.05). For both datasets left and left* / right and right* of we define two hypotheses :

H_0 : both datasets are from the same distribution.

H_a : both datasets are from a different distribution

The non parametric test Shapiro-wilk was applied to compare CR and Zcr value to investigates a significative difference between sample with and without mirrored bones.

- *Hypothesis 1 with and without pisiform*

Although the pisiform was not incorporate in the wrist for the modularity analysis because it was hardly reducing the sample of complete wrist, it was still present in the collection and scanned. Consequently, it was fair enough to include it in a small investigation on the hypothesis 1 only (hypothesis 1b Table 5).

By applying a Kruskall Wallis test we can compare independent sample to know if they come from the same distribution. This test was used on the covariance strength (Zcr) of samples left and right “ wrist* ”, “ wrist ”, and “ wrist with Pisiform ”. This last samples are composed by wrist* and wrist that are completed with pisiform.

5. RESULTS

ANOVA intra-observer errors test allows us to claim that each landmarks template are repeatable, allowing us to pursue our quantitative 3D geo-morphological analysis. Sexual dimorphism univariate test shows no significative difference between female and male individuals buried in the convent of Burgos. Results of the modularity test will be differentiated in later paragraph between the ones from the sample with mirrored bones and without mirrored bones.

5.1.DESCRIPTIVE ANALYSE

On average around 60 bones were scanned for each carpals (Figure 32), though the sample gathers more carpals from the distal row than from the proximal row (248 against 205 bones) (Figure 32). In general more left bones than right were scanned (217 against 236) (Figure 31). In total 453 carpals were scanned, 32 bones were broken (missing hamate's hamulus, trapezium bridge, part of articular facet) or altered (arthritis, osteoporosis) (Table 3: Table 3). 421 bones out of 453 were **well preserved**. Pisiform bones are the least numerous in both the right and left hand samples (16 and 15, respectively), whereas the left hamate is the most abundant in the left hand sample and the capitate in the right hand sample (38 and 33, respectively). It is worth noting that carpal bones are difficult to find due to their small size, taphonomy factors, rapid fragmentation and even excavation methodology errors. They also have a lower mass than other bones of the skeleton making the first to decompose.

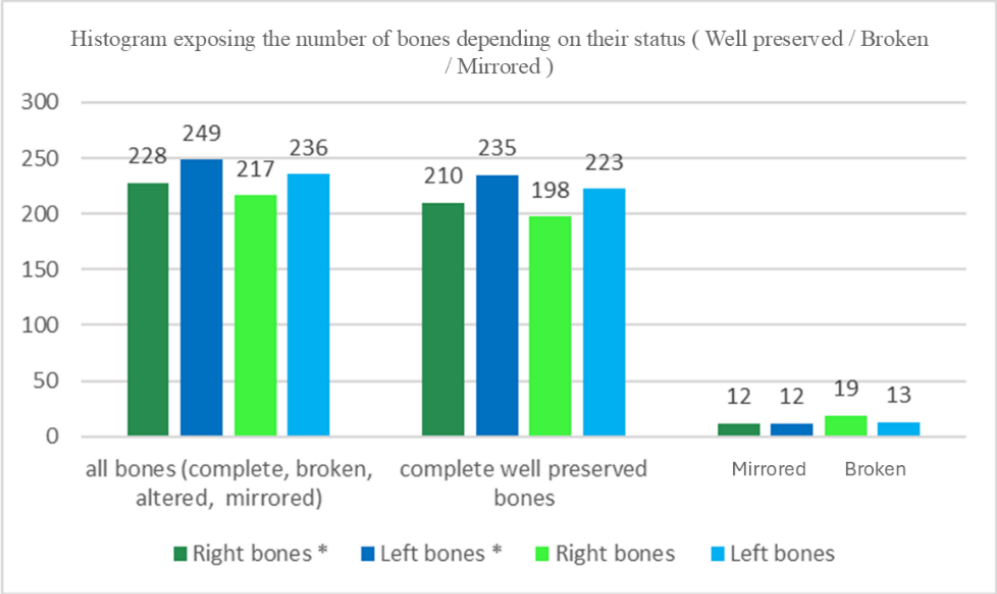

Figure 31: histogram of the carpal's quantity, (*) means that mirrored bones are included in the sample

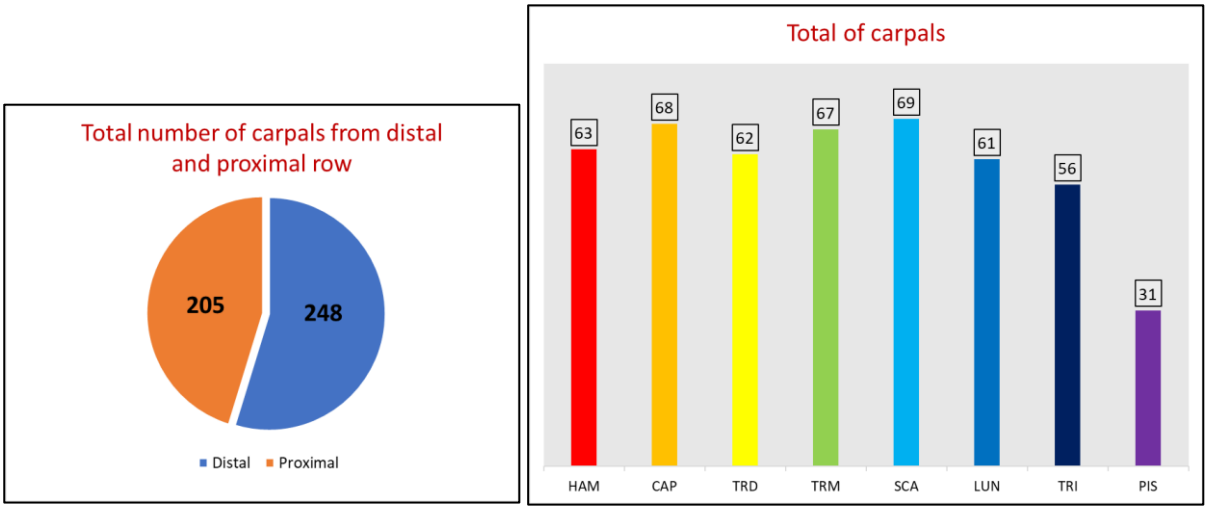

*Figure 32: **Left** distribution of carpals from proximal and distal row, **Right** histogram with the total number of each of the eight carpals*

➢ *Analysis of repeatability*

It results that there are no significative differences between the repeated set of landmarks (table of ANOVA test Pvalue>0.05 is presented in the annexes). Although trapezium Pvalue is closer to 0.05 (p=0.08) we will accept the no difference. This observation can be link with one high variability in the placement of the landmark number 9 which goes on the top of the tubercule of the trapezium that sometimes can be deformed or split into two high formations on the top of the tubercule.

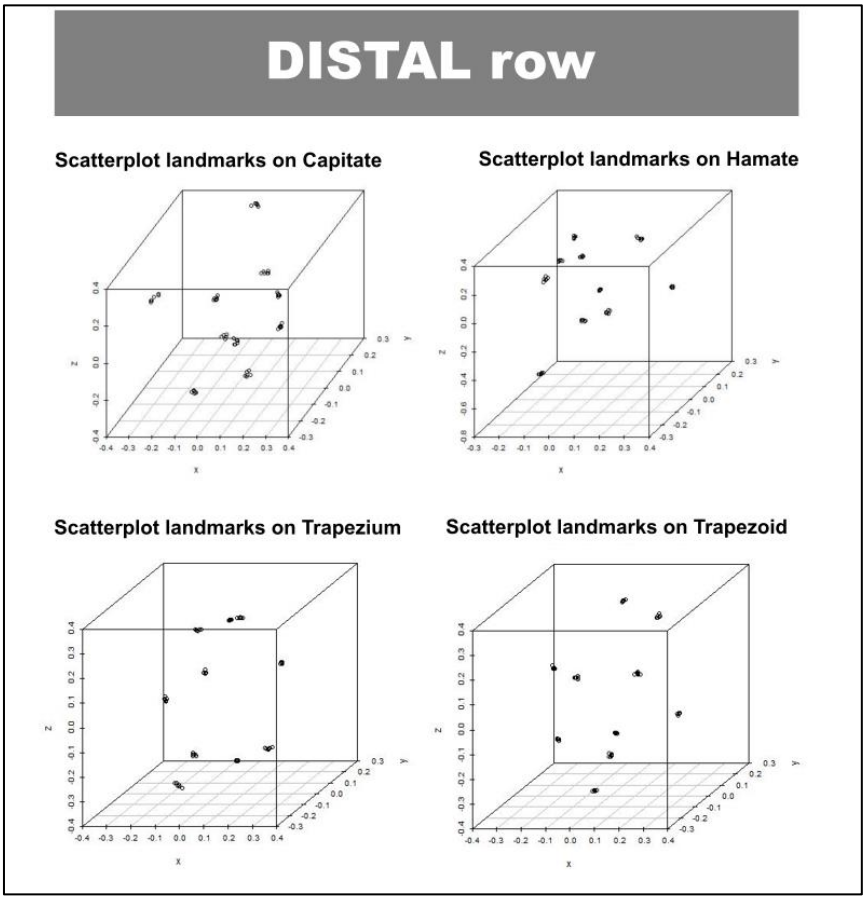

Figure 33: Scatterplot of the procrustes coordinates of the 10 landmarks on the four distal row carpals

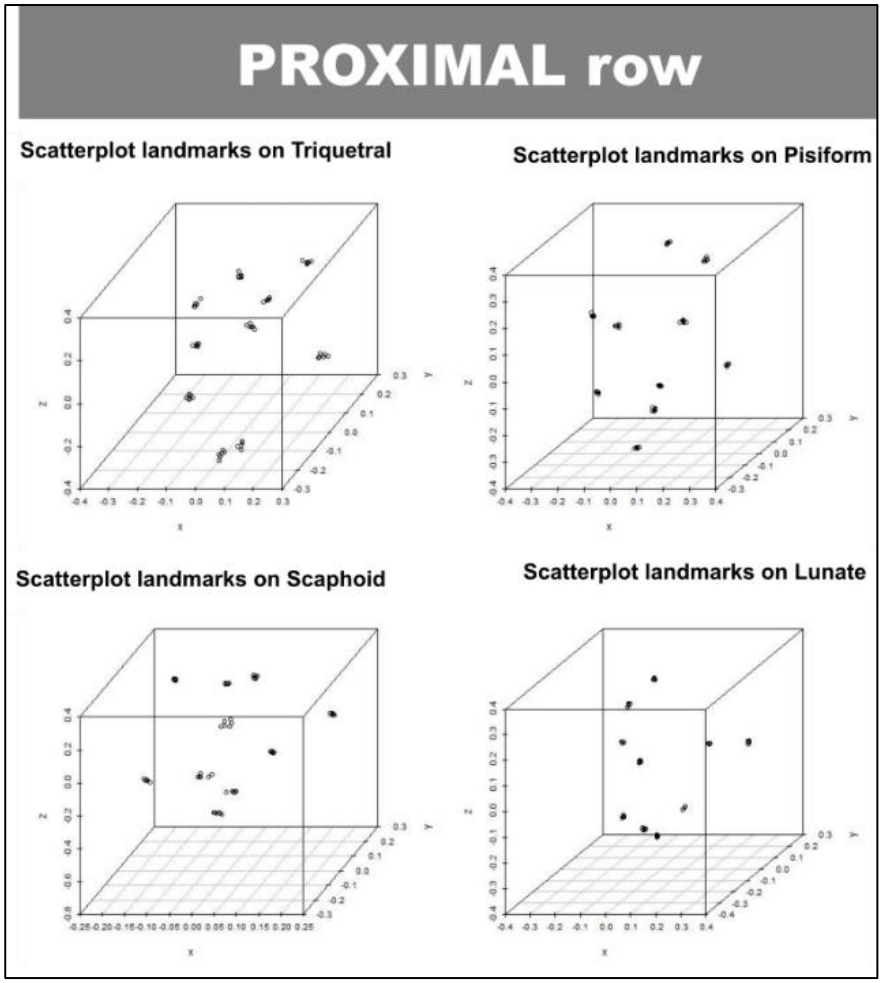

Figure 34: Scatterplot of the Procrustes coordinates of the 10 landmarks on the four proximal row carpals

- ***The effect of mirrored bones on modularity test***

Mann-Whitney statistic tests were conducted on modularity test's results Covariance and Zcr, in order to know if adding mirrored bones in the sample had a significative impact. H_o cannot be rejected, we observe that between right wrist and right wrist* samples there is no significative difference as well as in left wrist and wrist* samples (Table 6 Mann-Whitney test P value>0.05). The presence of mirrored bones in a sample doesn't have a significative effect on covariance value and Zcr value of a modularity test conducted.

Table 6: Pvalue of the non-parametric Mann-Whitney test between wrist and wrist sample's covariance and Zscore values*

Mann-Whitney test		RIGHT	LEFT
P value	**CR**	0,3	0,1
	Zcr	0,3	0,8

5.2.SEXUAL DIMORPHISM

Overall, females show a more narrowed central distribution (interquartile range) than males, except for the lunate and trapezoid (Figure 35). Despite the capitate distribution having outliers, it has the most narrowed central distribution among all carpals for both males and females. Approximately 75% of female capitates have their centroid size below the median of the males. On the contrary, 75% of female triquetrals have their centroid size above the median of the males, although the central distribution is broader in males than in females (Figure 35).

Males have larger centroid sizes for the hamate, capitate, and lunate compared to females, while the triquetral, scaphoid, and trapezium exhibit the opposite trend. In the lunate centroid size distribution, the median for males is above 75% of the centroid sizes for female individuals. For the scaphoid, approximately 70% of the centroid sizes in females are above the median centroid size of males. Although the median centroid size of the female trapezium is higher than that of the male individuals, 50% of the values around the female median fall within the male central distribution. Median of centroid size of the trapezoid are similar in male and female, while the central distribution of female is widely broader than in male. Indeed, the overall distribution of male trapezoid centroid size fall within the 50% value around the median of females. In general the maximum highest value of a centroid size is displayed in the male distribution (Figure 35). The non-parametric statistical test Mann-Whitney shows for the seven carpals a pvalue above 0.05 (Table 7).

Table 7: P-value of the non-parametric test Mann-Whitney between men and women carpals centroid size

Bone	Mann_Whitney	Pvalue
SCA	166	0,46
LUN	63	0,30
TRI	107	0,43
TRD	120	0,77
TRM	113	0,75
HAM	63	0,63
CAP	78	**0,0615**

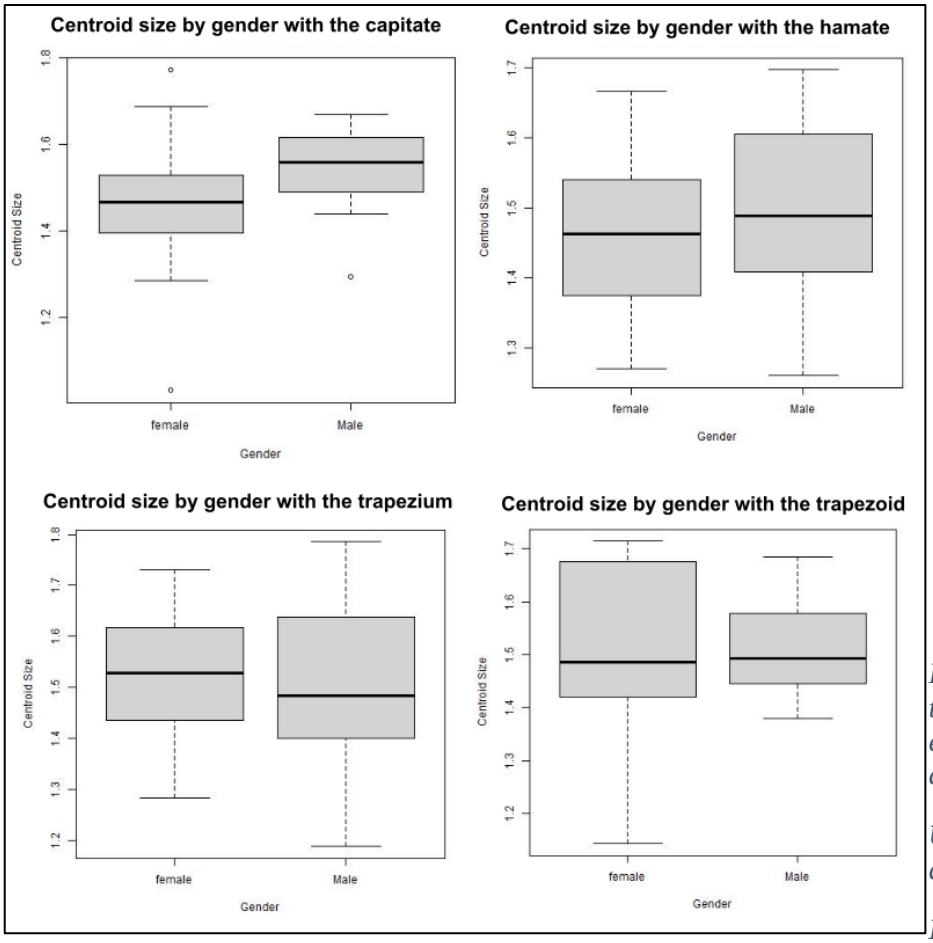

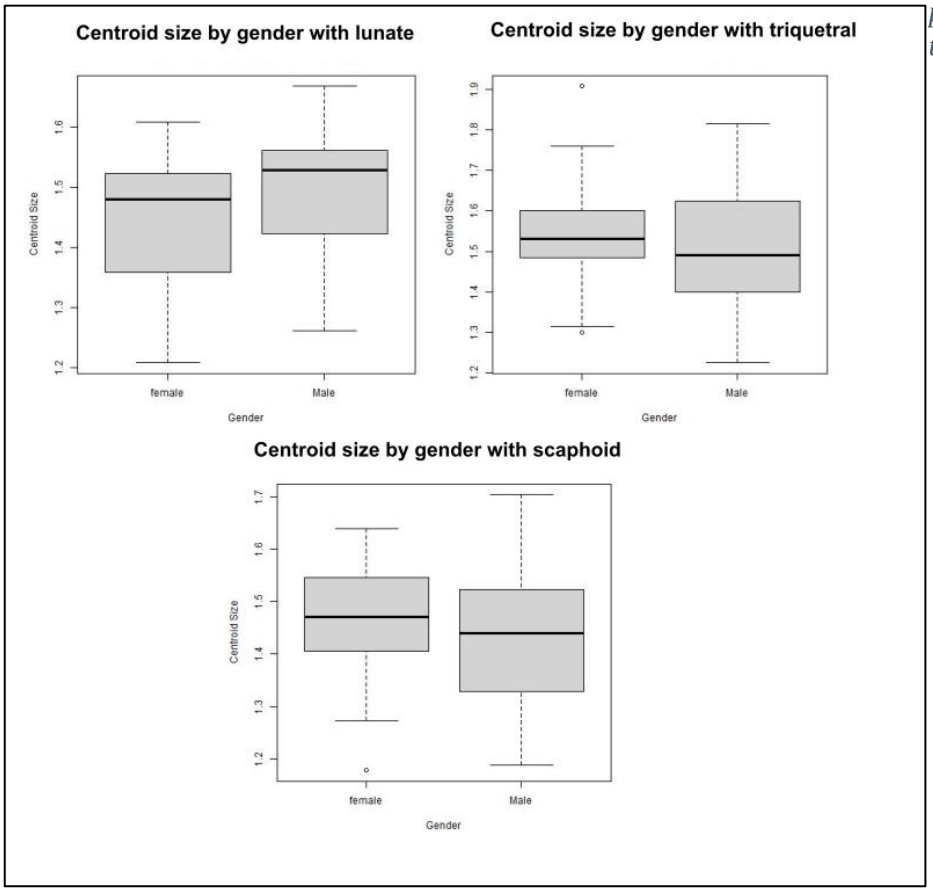

Figure 35: Boxplot of the centroid size for each carpal of women and men individuals.

***Up** carpals from distal row.*

***Down** carpals from proximal row except the pisiform.*

5.3.MODULARITY SIGNALS BETWEEN HYPOTHESES

From a general overview, we observe that all CR are significantly lesser than 1 (P values=0.001) (Table 9). It indicates the samples shows a strong modular signal regardless how bones were combined into modules. Then, in all the fourth sample (right, right*, left, left*) hypothesis 1 exhibited the largest negative Zcr (Figure 36). Which was significatively different from all others hypothesis (Zpairwise pvalue<0.05 table is presented in the annexes), except in the left and right wrist* samples. Indeed, in both of them there is no significative difference between H7 and H1 strength of covariance (effect size measure Zcr) (Zpairwise = 1,50 and 1,36 , pvalue>0.05).Moreover, all hypothesis with a configuration of 3 modules have the closer to 0 covariance ratio (Figure 37) but their Zcr are not significatively different between them (Zpairwise table in annexes).

Finally, all 8 hypotheses of left wrist without mirrored bones have modular signal higher in every sample (Figure 38). However, there is no significative difference in covariance and Zcr score between a sample with and without mirrored carpals (p value of mann whitney test >0.05 Table 6). Thanks to a Kruskall wallis test we observe that samples wrist, wrist* and wrist with Pisiform left and right aren't significatively differing regarding their effect size measures (Zcr) (Table 8). Thus, there is no significative difference between Zcr of hypothesis 1 from the different samples.

Table 8: Results of modularity test conducted on hypothesis 1 solely. For each hand side there are sample without mirrored bones, with mirrored bones and with mirrored + pisiform. ***Down*** *is non parametric test Kruskall-Wallis results*

H1 hypothesis				
	Hypothesis	**Covariance**	**Zcr**	**P.value**
RIGHT	Right wrist without mirorred	0,74	-9,04	0,001
	Right wrist*	0,68	-7,76	0,001
	Right wrist with PISIFORM	0,79	-9,25	0,001
LEFT	Left wrist without mirorred	0,76	-9,21	0,001
	Left wrist*	0,69	-8,18	0,001
	Left wrist with PISIFORM	0,82	-8,88	0,001
	Kruskal wallis test	**Satistic** 5	**Pvalue** 0,415880187	

Table 9: Covariance and Zcr result from modularity test of the 8 hypotheses made on the four different samples. ***Up*** *is the right wrist,* ***Down*** *is the left wrist.*

modularity test results (*= with mirrored bones)

RIGHT

Right wrist unmirrored N=12

Hypothesis	Covariance	Zcr	P.value
H1	0,74	-9,04	0,001
H2	0,89	-6,21	0,001
H3	0,85	-7,40	0,001
H4	0,87	-6,81	0,001
H5	0,86	-7,18	0,001
H6	0,94	-4,20	0,001
H7	0,83	-6,17	0,001
H8	0	0	0

Right wrist* N=19

Hypothesis	Covariance	Zcr	P.value
H1	0,68	-7,76	0,001
H2	0,85	-6,17	0,001
H3	0,81	-6,76	0,001
H4	0,85	-5,89	0,001
H5	0,83	-6,25	0,001
H6	0,92	-3,90	0,001
H7	0,78	-5,70	0,001
H8	0	0	0

LEFT

Left wrist unmirrored N=11

Hypothesis	Covariance	Zcr	P.value
H1	0,76	-9,21	0,001
H2	0,91	-6,65	0,001
H3	0,92	-6,19	0,001
H4	0,90	-6,88	0,001
H5	0,88	-7,50	0,001
H6	0,96	-3,90	0,001
H7	0,88	-5,89	0,001
H8	0	0	0

Left wrist* N=20

Hypothesis	Covariance	Zcr	P.value
H1	0,69	-8,18	0,001
H2	0,88	-6,28	0,001
H3	0,85	-7,06	0,001
H4	0,83	-7,42	0,001
H5	0,83	-7,60	0,001
H6	0,90	-5,36	0,001
H7	0,82	-5,88	0,001
H8	0	0	0

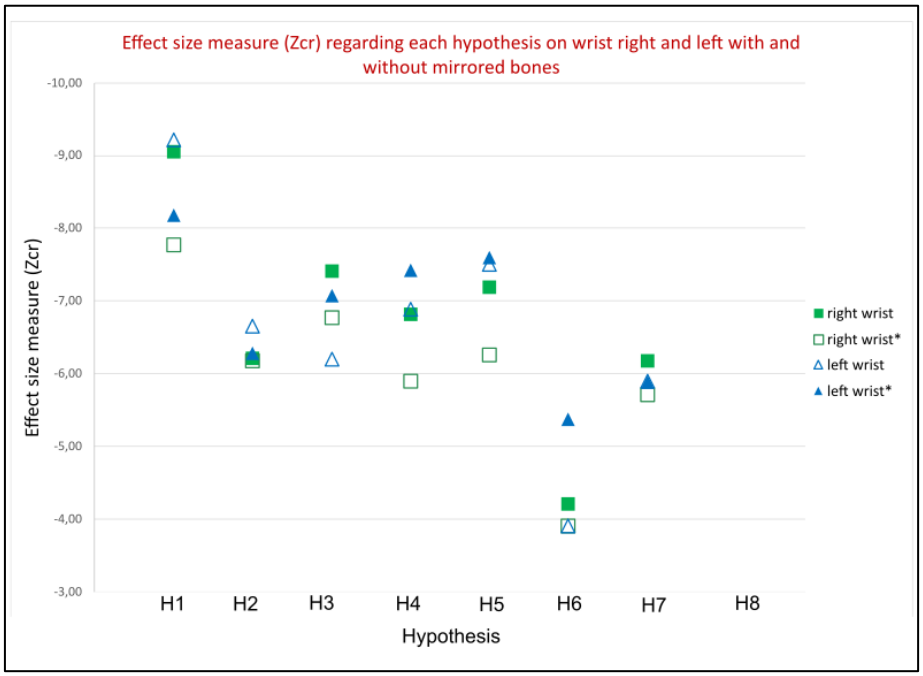

Figure 36: Effect size measure (Zcr) of each hypothesis from the four samples (legend on the right of the figure)

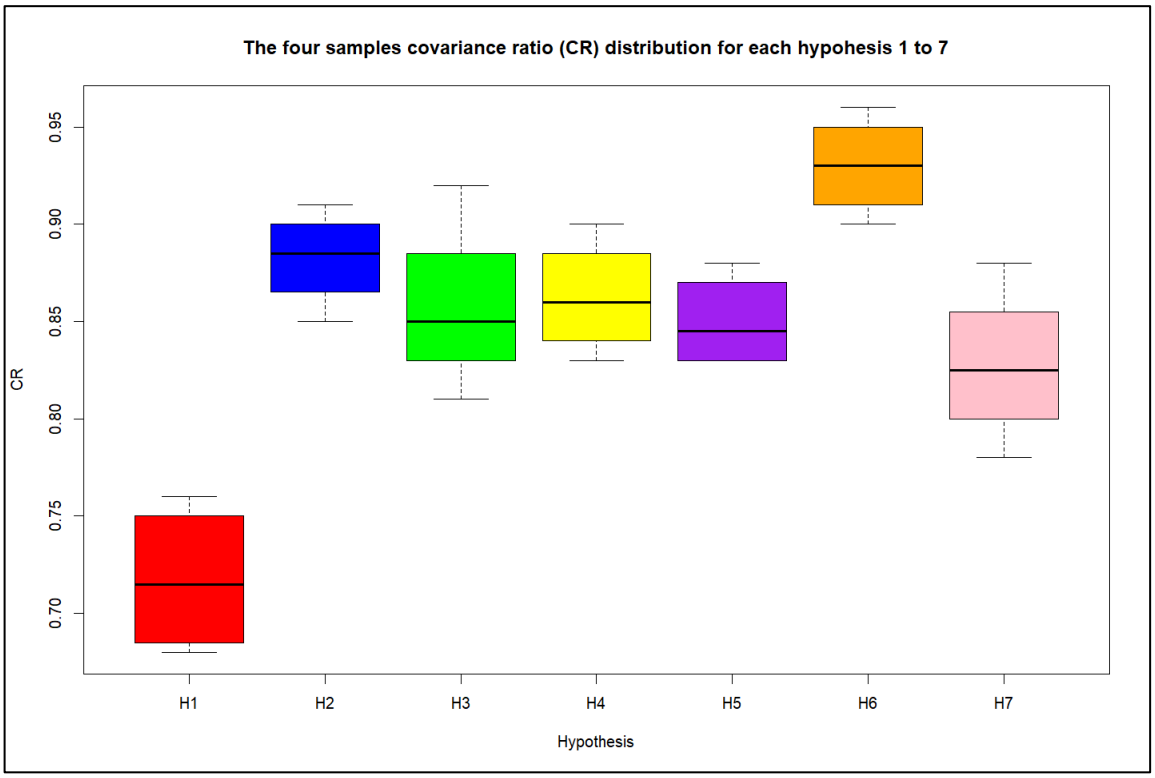

Figure 37: Boxplot of the CR of each hypothesis except H8 that doesn't appears because it is zero

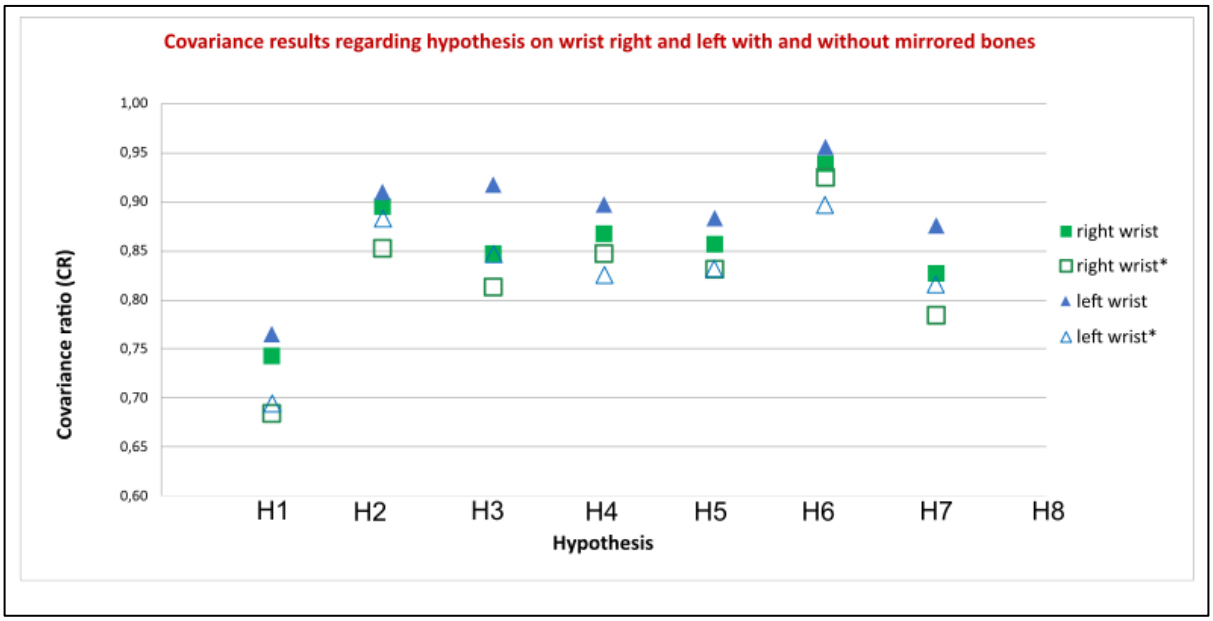

Figure 38: Covariance (CR) of each hypothesis from the four samples (legend on the right of the figure)

5.3.1. *In sample without mirrored bones*

- *Right wrist*

From the samples of right wrist that doesn't contains mirrored bones, it appears that H7 followed H1 with the second-highest modular signal. The Zcr of H7 is smaller than that of H2, H3, H4, and H5, yet these differences were not significant. Then, H6 shows the weakest modular signal (CR) that is significatively closer to 1 than any others hypothesis (Table 10). Additionally, the Zcr of H6 is significantly the smallest negative value among all hypotheses H2(Zpairwise =2.74 , pvalue = 0.06) H1(Zpairwise = 5.27 , pvalue = 1,3E-07) H4(Zpairwise = 2.24 , pvalue = 0.025) , H5 (Zpairwise = 2.51, pvalue = 0.012) , H7(Zpairwise = 2.85 , pvalue = 0.04) H8(Zpairwise = 4.19 , pvalue = 0.0000),except for H3 (Zpairwise =1.41 , p-value = 0.156).

Table 10: modularity test results of the eight hypotheses of the sample with carpals right unmirrored

Right wrist unmirrored N=12			
Hypothesis	**Covariance**	**Zcr**	**P.value**
H1	0,74	-9,04	0,001
H2	0,89	-6,21	0,001
H3	0,85	-7,40	0,001
H4	0,87	-6,81	0,001
H5	0,86	-7,18	0,001
H6	0,94	-4,20	0,001
H7	0,83	-6,17	0,001
H8	0	0	0

- *Left wrist.*

In the samples of left wrists without mirrored bones we can see that covariance values are remarkably close to one compared to other samples. H6 shows the weakest modular signal (CR) and its covariance value is significantly closer to 1 than any other hypothesis (Table 11). Moreover, its Zcr is significantly the smallest between H1 (Zpairwise = 5.56, p-value = 0.0000), H4 (Zpairwise = 2.45, p-value = 0.014), H5 (Zpairwise = 2.91, p-value = 0.004), H7 (Zpairwise = 2.84, p-value = 0.004), and H8 (Zpairwise = 3.90, p-value = 0.00000). Additionally, it appears that H5 and H7 have the same covariance value, yet their Zcr score was larger for H5, although

the difference was not significant. Also, H5 has the second-highest modular signal and the second-largest negative value of Zcr (Figure 36), yet this difference was not significant between the other hypotheses.

Table 11: modularity test results of the eight hypotheses of the sample with carpals left unmirrored

Left wrist unmirrored N=11			
Hypothesis	**Covariance**	**Zcr**	**P.value**
H1	0,76	-9,21	0,001
H2	0,91	-6,65	0,001
H3	0,92	-6,19	0,001
H4	0,90	-6,88	0,001
H5	0,88	-7,50	0,001
H6	0,96	-3,90	0,001
H7	0,88	-5,89	0,001
H8	0	0	0

5.3.2. In sample with mirrored bones

- *Right wrist**

Hypothesis H1 exhibits the covariance value closest to zero, followed by H7 (Figure 38). However, when examining the standardized Zcr scores, H7 does not significantly differ from any hypothesis except H8 (no module hypothesis) and H6 (Zpairwise =2.54 , p-value = 0.011). Also, H7 has a significative higher modular signal (CR) compared to H6, with a Zcr score significantly higher in negative value (respectively 5,70 and 3,90). The covariance of H6 (Table 12 CR= 0,92) is closest to 1, indicating the weakest modular signal, with significant differences in their effect size measure observed only when compared to H1 (Zpairwise=4,18 , pvalue= 0.00),H2 (Zpairwise =2.39, pvalue = 0.01), H7(Zpairwise =2.54 , p-value = 0.011) , and H8 (no module hypothesis). Covariance values for H2, H3, H4, and H5 range from 0.81 to 0.83, which are higher than those of H1 and H7 but lower than that of H6. However, the pairwise differences in their Zcr scores are not significant, except when compared to H1 (H2 z pairwise = 2.86, pvalue = 0.03 ; H3 z pairwise = 2,09, pvalue = 0.004 ; H4 z pairwise = 2.52, pvalue = 0.01 ; H5 zpairwise =2.31, pvalue = 0.02).

Table 12: modularity test results of the eight hypotheses of the sample with carpals right unmirrored and mirrored

Right wrist* N=19			
Hypothesis	**Covariance**	**Zcr**	**P value**
H1	0,68	-7,76	0,001
H2	0,85	-6,17	0,001
H3	0,81	-6,76	0,001
H4	0,85	-5,89	0,001
H5	0,83	-6,25	0,001
H6	0,92	-3,90	0,001
H7	0,78	-5,70	0,001
H8	0	0	0

- *Left wrist**

Hypothesis H1 exhibited the minimum covariance value and the highest negative Zcr score (Figure 38 ; Figure 36), although the difference between H1 and H7 is not significant (Zpairwise = 1.50 , pvalue = 0.133). Both H6 and H7 have smaller negative Zcr values (Table 13). H7 has a higher modular signal than H6, although their Zpairwise comparison does not show a significant difference (Zpairwise = 1,79, pvalue = 0.07).

Table 13: modularity test results of the eight hypotheses of the sample with carpals left unmirrored and mirorred

Left wrist* N=20			
Hypothesis	**Covariance**	**Zcr**	**P value**
H1	0,69	-8,18	0,001
H2	0,88	-6,28	0,001
H3	0,85	-7,06	0,001
H4	0,83	-7,42	0,001
H5	0,83	-7,60	0,001
H6	0,90	-5,36	0,001
H7	0,82	-5,88	0,001
H8	0	0	0

6. DISCUSSION AND FUTURES PERSPECTIVE

This study's aims were to present different modular configuration among the seven carpals of Homo sapiens and find the best fit that describe covariation patterns within the wrist, by using geomorphometry approach on a digital collection created especially for this work. Additionally, sexual dimorphism in carpals centroid size were analysed.

6.1.SEXUAL DIMORPHISM

Sexual dimorphism was investigated using the centroid size of Procrustes coordinates (i.e., values from the "gpagen" function in R) of seven carpals (triquetral, lunate, scaphoid, hamate, trapezoid, trapezium, and capitate). A non-parametric test was applied to the distribution of male and female centroid sizes of carpals from left wrists. Although carpals are generally larger in males, the statistical comparison did not yield significant differences between male and female distributions for the seven carpals (Table 7). However, this comparison might be underpowered due to the small sample size (Table 1), which could be addressed in future analyses with larger datasets. Additionally, the centroid size used in this sexual dimorphism study might be affected by the number and placement of landmarks. The protocol proposed earlier in the study includes a set of 10 landmarks for each carpal, which could be refined and improved for accuracy by incorporating semi-landmarks.
Furthermore, only left carpals were analysed, but a more comprehensive study could include carpals from the right wrist. It is important to note that most Homo sapiens are right-handed; thus, the right wrists of individuals buried in the Convent of Burgos might show shapes influenced by daily tasks, potentially affecting the cortical surfaces of the carpals.

Research on sexual dimorphism in forensic collections has shown promising results for the hand. Sex estimation within upper limbs has been investigated in Thai populations (Barnes et al., 2020), Eskimos from Alaska (Bennett, 1981), and the Hadza population in Tanzania (Hiernaux & Hartono, 1980), where wrist and palm breadth were studied as high criterion for sex estimation. Loesch et al. (1992) evaluated wrist breadth as the second most dimorphic

anthropometric variable in European and Australian populations. Thus, the wrist remains a promising area for sexual dimorphism investigations in forensic collections.

6.2.MODULARITY WITHIN THE WRIST

We aimed to describe the modular pattern in the wrist of Homo sapiens and identify the best fit for covariation among kinematic model hypotheses. Our analysis revealed that adding mirrored bones in sample did not significantly influence the modularity results (Table 6). However, the number of pisiforms was clearly too low, but we showed that its presence did not influence the modularity results of hypothesis 1 only (Table 8). As the kinematic hypothesis used here were not including it, future studies should reconsider making *a priori* modular structure with pisiform, though it is hardly rare to find this small bone during excavation and in collections.

The covariation ratio was used to evaluate how changes in one carpal are associated with changes in each of the other articulated carpals, and we also examined the standardized effect size to statistically compare covariance ratios between them. The landmark template proposed have been proved to be scientifically correct and can be used in future morphological integration examination in carpal bones; The analysis of modularity within the wrist revealed that the best fit is Hypothesis 1 (Figure 37), indicating that each carpal functions as its own modular unit. This finding resonates with the work of Bucchi et al (2020) who compared modularity within the wrist in non-human primates and Homo sapiens and observed the same hypothesis 1 as the highest modular signal in Homo sapiens. Hypothesis 1 resulting as the best fit for modules configuration (Figure 37) is confirming a high independency in shape variation between carpals as it is observed in O.J.Lewis et al. (1972) Corruccini et al. (1978), and Kivell et al. (2013) works, who noted a complex mosaic patterns of morphological evolution that underlies the hominoid wrist. Hypotheses that propose separation into two modules did not provide the best fit. Then, hypothesis 7, which describes the carpal's kinematics called "screw vice"(the distal row is one modules, than lunate and triquetral are the second module and the scaphoid is the third module on itself) emerged as the second-best fit in modular configuration (Figure 36 ; Figure 37). It can be interpreted as, the presence of a high concentration of integration within the distal row and weak integration between the distal row and scaphoid and between the distal

row and the triquetrolunate module. In an anatomical point of view, the carpals of the distal row are very bound to each other by strong ligaments and are seen as one functional units (Eschweiler et al., 2022). This aligns with studies of Akhbari et al. (2019), Brinkhorst et al. (2022), Norman et al. (2023), and Ruby et al. (1988), which suggest that the distal row may function “as a rigid unit with little relative motion between the bones” (Norman et al., 2023, p. 5).

6.3.FUTURES PERSPECTIVE

Caution is advised in interpreting modularity : performing a Generalized Procrustes Analysis (GPA) with the “within method” reduces the appearance of covariation inflation, and the proposed hypotheses might inherently favor Hypothesis 1. Additionally, geomorphometry technic could be improve with a more detailed landmark configuration, the use of semi-landmark as well as a different statistical approach than the CR presented here. Also, sexual dimorphism could be investigated looking other parameters than the centroid size such as the individual carpal volume normalized with total carpus complex volume, and the palmar and wrist breadth.

Further analysis involving statistical comparisons between integration in Homo sapiens carpals and fossil hominids would be valuable by mixing hypothesis of modular configuration based on kinematic observations, with observations based on anatomic and wrist growth development. The collection of hand bones of the Dominican convent still has some bones to scan that could expand the study sample. Additionally, a matrix with 11 hypotheses would provide 1 hypothesis for each pair of carpals in articulation (one module for each carpal on itself and one module for two carpals in articulation). From this matrix more function from the GEOMORPH package in R could be applied and partial least square approach could be conducted. Finally, the observation made in this thesis work can be used as an actual reference for future analysis and comparison with non-human extinct primates’ carpals in order to investigate phylogenetic evolution evidence, manual ability or suspensory behaviour.

7. CONCLUSION

The aim of this master thesis was to study Homo sapiens carpals bones by looking for sexual dimorphism in shape, and investigating modularity within the wrist. It is the first time the seven carpals (the wrist without the pisiform) were used to acquire the best modular configuration that describes the covariation patterns within the wrist. The study involves the scanning process of the bones, placing virtual anthropology at the core of this research. The main conclusions are the following :

Firstly, inside the San Pablo population no sexual dimorphism in carpals shape was observed, yet only one parameter was used (centroid size from Procrustes coordinates). In a new study the protocol proposed could be reuse to look for sexual dimorphism throughout wrist breadth parameters with an expand sample. Then, regarding modularity investigation, we showed that mirrors bones can be included in modularity test without influencing results. Our main conclusion is that defining each Homo sapiens carpals as a module by themselves is a modular configuration that describes best covariation pattern within the wrist. We conclude that they covaries mainly with themselves, though with other carpals to a lesser degree. It could be related with the high morphological independency of wrist bones. However, the screw-vice kinematic theory was the second best fit for modular configuration and could be part of a further investigation to look for modular signal with this hypothesis in others Hominoid species. High-tech digital tools and software have significantly enhanced the accuracy of our work and opened up countless research possibilities, underscoring the central role of digital anthropology today. However, it is essential to remember that these tools can only produce meaningful results when used with actual fossils.

8. REFERENCES

Abdelhady, A. A., Seuss, B., Jain, S., Abdel-Raheem, K. H. M., Elsheikh, A., Ahmed, M. S., Elewa, A. M. T., & Hussain, A. M. (2024). New and emerging technologies in paleontology and paleobiology : A horizon scanning review. *Journal of African Earth Sciences*, *210*, 105155. https://doi.org/10.1016/j.jafrearsci.2023.105155

Adams, D. C. (2016). Evaluating modularity in morphometric data : Challenges with the RV coefficient and a new test measure. *Methods in Ecology and Evolution*, *7*(5), 565-572. https://doi.org/10.1111/2041-210X.12511

Adams, D. C., & Collyer, M. L. (2019). Comparing the strength of modular signal, and evaluating alternative modular hypotheses, using covariance ratio effect sizes with morphometric data. *Evolution*, *73*(12), 2352-2367. https://doi.org/10.1111/evo.13867

L. Aiello & C. Dean 1991, *An introduction to human evolutionnary anatomy,* Academic Press London

A.Peña, 2018. *Patterns of Integration and Modularity in the Hominoid Wrist,* (Master thesis) Arizona State University

Balzeau, A., Crevecoeur, I., Rougier, H., Froment, A., Gilissen, E., Grimaud-Hervé, D., Mennecier, P., & Semal, P. (2010). Applications of imaging methodologies to paleoanthropology : Beneficial results relating to the preservation, management and development of collections. *Comptes Rendus Palevol*, *9*(6), 265-275. https://doi.org/10.1016/j.crpv.2010.07.006

Bardo, A., Cornette, R., Borel, A., & Pouydebat, E. (2017). Manual function and performance in humans, gorillas, and orangutans during the same tool use task. *American Journal of Physical Anthropology*, *164*(4), 821-836. https://doi.org/10.1002/ajpa.23323

Bardo, A., Dunmore, C. J., Cornette, R., & Kivell, T. L. (2023). Morphological integration and shape covariation between the trapezium and first metacarpal among extant hominids. *American Journal of Biological Anthropology*, ajpa.24800. https://doi.org/10.1002/ajpa.24800

Bardo, A., Moncel, M.-H., Dunmore, C., Kivell, T., Pouydebat, E., & Cornette, R. (2020). The implications of thumb movements for Neanderthal and modern human manipulation. *Scientific Reports*, *10*, 19323. https://doi.org/10.1038/s41598-020-75694-2

Bardo, A., Town, K., Kivell, T. L., Donati, G., Ballieux, H., Stamate, C., Edginton, T., & Forrester, G. S. (2022). The Precision of the Human Hand : Variability in Pinch Strength and Manual Dexterity. *Symmetry*, *14*(1), 71. https://doi.org/10.3390/sym14010071

Barnes, A. E., Case, D. T., Burnett, S. E., & Mahakkanukrauh, P. (2020). Sex estimation from the carpal bones in a Thai population. *Australian Journal of Forensic Sciences*, *52*(6), 665-680. https://doi.org/10.1080/00450618.2019.1620856

Bennett, K. A. (1981). On the expression of sex dimorphism. *American Journal of Physical Anthropology*, *56*(1), 59-61. https://doi.org/10.1002/ajpa.1330560106

Bird, E. E., Kivell, T. L., Dunmore, C. J., Tocheri, M. W., & Skinner, M. M. (2023). Trabecular bone structure of the proximal capitate in extant hominids and fossil hominins with implications for midcarpal joint loading and the dart-thrower's motion. *American Journal of Biological Anthropology*, ajpa.24824. https://doi.org/10.1002/ajpa.24824

Bird, E. E., Kivell, T. L., & Skinner, M. M. (2022). Patterns of internal bone structure and functional adaptation in the hominoid scaphoid, lunate, and triquetrum. *American Journal of Biological Anthropology*, *177*(2), 266-285. https://doi.org/10.1002/ajpa.24449

Bird, E., Kivell, T., & Skinner, M. (2021). Cortical and trabecular bone structure of the hominoid capitate. *Journal of Anatomy*, *239*. https://doi.org/10.1111/joa.13437

Bookstein, F. L. (1991). *Morphometric tools for landmark data: Geometry and biology*. Cambridge University Press

Bryce, T. H. (1896a). Certain Points in the Anatomy and Mechanism of the Wrist-Joint Reviewed in the Light of a Series of Röntgen Ray Photographs of the Living Hand. *Journal of Anatomy and Physiology*, *31*(Pt 1), 59-79.

Bryce, T. H. (1896b). Certain Points in the Anatomy and Mechanism of the Wrist-Joint Reviewed in the Light of a Series of Röntgen Ray Photographs of the Living Hand. *Journal of Anatomy and Physiology*, *31*(Pt 1), 59-79.

Bucchi, A. (2020). *Approaches for assessing whether the human hand evolved by natural selection in adaptation to stone tool use*. https://doi.org/10.13140/RG.2.2.28567.60327

Bucchi, A., Püschel, T., & Lorenzo, C. (2022). Modularity of the wrist in extant hominines. *Anthropologischer Anzeiger*, *80*. https://doi.org/10.1127/anthranz/2022/1558

Cardini, A. (2019). Integration and Modularity in Procrustes Shape Data : Is There a Risk of Spurious Results? *Evolutionary Biology*, *46*(1), 90-105. https://doi.org/10.1007/s11692-018-9463-x

Clark, J. T., Slator, B. M., Bergstrom, A., Larson, F., Frovarp, R., Landrum, J. E., & Perrizo, W. (2001). Preservation and access of cultural heritage objects through a digital archive network for anthropology. *Proceedings Seventh International Conference on Virtual Systems and Multimedia*, 28-38. https://doi.org/10.1109/VSMM.2001.969652

Conroy, G. C., & Vannier, M. W. (1984). Noninvasive three-dimensional computer imaging of matrix-filled fossil skulls by high-resolution computed tomography. *Science (New York, N.Y.)*, *226*(4673), 456-458. https://doi.org/10.1126/science.226.4673.456

Corruccini, R. S. (1987). Shape in morphometrics : Comparative analyses. *American Journal of Physical Anthropology*, *73*(3), 289-303. https://doi.org/10.1002/ajpa.1330730303

Destot, É. (2006). The Classic : Injuries of the Wrist: A Radiological Study. *Clinical Orthopaedics and Related Research*, *445*, 8-14. https://doi.org/10.1097/01.blo.0000205896.83114.05

Dunmore, C. J., Bachmann, S., Synek, A., Pahr, D. H., Skinner, M. M., & Kivell, T. L. (2023). The deep trabecular structure of first metacarpals in extant hominids. *American Journal of Biological Anthropology*, ajpa.24695. https://doi.org/10.1002/ajpa.24695

Dunmore, C. J., Bardo, A., Skinner, M. M., & Kivell, T. L. (2020). Trabecular variation in the first metacarpal and manipulation in hominids. *American Journal of Physical Anthropology*, *171*(2), 219-241. https://doi.org/10.1002/ajpa.23974

Eschweiler, J., Li, J., Quack, V., Rath, B., Baroncini, A., Hildebrand, F., & Migliorini, F. (2022). Anatomy, Biomechanics, and Loads of the Wrist Joint. *Life*, *12*(2), Article 2. https://doi.org/10.3390/life12020188

Galletta, L., Stephens, N. B., Bardo, A., Kivell, T. L., & Marchi, D. (2019a). Three-dimensional geometric morphometric analysis of the first metacarpal distal articular surface in humans, great apes and fossil hominins. *Journal of Human Evolution*, *132*, 119-136. https://doi.org/10.1016/j.jhevol.2019.04.008

Galletta, L., Stephens, N. B., Bardo, A., Kivell, T. L., & Marchi, D. (2019b). Three-dimensional geometric morphometric analysis of the first metacarpal distal articular surface in humans, great apes and fossil hominins. *Journal of Human Evolution*, *132*, 119-136. https://doi.org/10.1016/j.jhevol.2019.04.008

Gaskin, C. M., Kahn, S. L., Bertozzi, J. C., & Bunch, P. M. (2011). *Skeletal Development of the Hand and Wrist : A Radiographic Atlas and Digital Bone Age Companion*. Oxford University Press. https://doi.org/10.1093/med/9780199782055.001.0001

Gerhard W.Weber & Fred L.Bookstein. (2010). *Virtual Anthropology* (1re éd.). Springer Vienna. https://link.springer.com/book/9783211486474

Gilsanz, V., & Ratib, O. (2005). *Hand bone age : A digital atlas of skeletal maturity; [CD-ROM included]*. Springer.

Gorjanović-Kramberger, D. (1906). *Der diluviale Mensch von Krapina in Kroatien : Ein beitrag zur Paläoanthropologie*. C. W. Kreidel.

Guipert, G., Subsol, G., Jessel, J.-P., Hervé, D., & Mafart, B. (2003, January 1). The FOVEA project: A new look at human past. In *Proceedings of the Ninth International Conference on Virtual Systems and Multimedia (VSMM 2003)* (pp. 42-48). Montreal, Canada.

Hammer, Ø., & Harper, D. A. T, 2006. *Paleontological Data Analysis*, Blackwell Publishing Ltd UK

Hiernaux, J., & Hartono, D. B. (1980). Physical measurements of the adult Hadza of Tanzania. *Annals of Human Biology*, *7*(4), 339-346. https://doi.org/10.1080/03014468000004411

Jones, F. W. (Frederic W. (avec University of California Libraries). (1920). *The principles of anatomy as seen in the hand*. London, J. & A. Churchill. http://archive.org/details/principlesofanat00jonerich

Jungers, W. L., Falsetti, A. B., & Wall, C. E. (1995). Shape, relative size, and size-adjustments in morphometrics. *American Journal of Physical Anthropology*, *38*(S21), 137-161. https://doi.org/10.1002/ajpa.1330380608

Karakostis, F. A., Hotz, G., Tourloukis, V., & Harvati, K. (2018). Evidence for precision grasping in Neandertal daily activities. *Science Advances*, *4*(9), eaat2369. https://doi.org/10.1126/sciadv.aat2369

Karakostis, F. A., & Lorenzo, C. (2016). Morphometric patterns among the 3D surface areas of human hand entheses. *American Journal of Physical Anthropology*, *160*(4), 694-707. https://doi.org/10.1002/ajpa.22999

Kivell, T. L. (2016). A review of trabecular bone functional adaptation : What have we learned from trabecular analyses in extant hominoids and what can we apply to fossils? *Journal of Anatomy*, *228*(4), 569-594. https://doi.org/10.1111/joa.12446

Kivell, T. L. (2021). Human evolution : Thumbs up for efficiency. *Current Biology*, *31*(6), R289-R291. https://doi.org/10.1016/j.cub.2021.02.021

Kivell, T. L., Baraki, N., Lockwood, V., Williams-Hatala, E. M., & Wood, B. A. (2022). Form, function and evolution of the human hand. *American Journal of Biological Anthropology*, *n/a*(n/a). https://doi.org/10.1002/ajpa.24667

Klingenberg, C. P. (2009). Morphometric integration and modularity in configurations of landmarks : Tools for evaluating a priori hypotheses. *Evolution & Development*, *11*(4), 405-421. https://doi.org/10.1111/j.1525-142X.2009.00347.x

Klingenberg, C. P. (2014). Studying morphological integration and modularity at multiple levels : Concepts and analysis. *Philosophical Transactions of the Royal Society B: Biological Sciences*, *369*(1649), 20130249. https://doi.org/10.1098/rstb.2013.0249

Kralick, A., & Tocheri, M. (2014). *A 3D quantitative comparative analysis of wrist morphology among western and eastern gorillas*.

Lewis 1989, *Book Functional Morphology of the Evolving Hand and Foot,* Oxford Science Publications

Lichtman, D. M., Schneider, J. R., Swafford, A. R., & Mack, G. R. (1981). Ulnar midcarpal instability—Clinical and laboratory analysis. *The Journal of Hand Surgery*, *6*(5), 515-523. https://doi.org/10.1016/S0363-5023(81)80115-3

Lockwood, Victoria A (2018) *Biomechanics of the human hand during suspensory locomotion: a combined pressure and kinematic approach.* Master of Science by Research (MScRes) thesis, University of Kent.

Loesch, D. Z., Lafranchi, M., & Huggins, R. (1992). A new anthropometric scale for discrimination between sexes. *Annals of Human Biology*, *19*(2), 177-184. https://doi.org/10.1080/03014469200002052

MacConaill, M. A. (1941). The mechanical anatomy of the carpus and its bearings on some surgical problems. *Journal of Anatomy*, *75*(Pt 2), 166-175.

Marzke, M. (2013). Tool making, hand morphology and fossil hominins. *Philosophical transactions of the Royal Society of London. Series B, Biological sciences*, *368*, 20120414. https://doi.org/10.1098/rstb.2012.0414

Marzke, M. W. (1971). Origin of the human hand. *American Journal of Physical Anthropology*, *34*(1), 61-84. https://doi.org/10.1002/ajpa.1330340106

Moritomo, H., Murase, T., Goto, A., Oka, K., Sugamoto, K., & Yoshikawa, H. (2004). Capitate-based kinematics of the midcarpal joint during wrist radioulnar deviation : An in vivo three-dimensional motion analysis. *The Journal of Hand Surgery*, *29*(4), 668-675. https://doi.org/10.1016/j.jhsa.2004.04.010

Morley, J., Bucchi, A., Lorenzo, C., & Püschel, T. A. (2020). *Characterizing the body morphology of the first metacarpal in the Homininae using 3D geometric morphometrics*. https://doi.org/10.1101/2020.04.30.070326

Napier, J. R. (1956). THE PREHENSILE MOVEMENTS OF THE HUMAN HAND. *The Journal of Bone & Joint Surgery British Volume*, *38-B*(4), 902-913. https://doi.org/10.1302/0301-620X.38B4.902

Norman, E., Mistry, M. R., Lalone, E., & Suh, N. (2023). A Kinematic Analysis of Wrist and Carpal Function Using Four-Dimensional Computed Tomography Technology : A Dynamic Perspective. *The Journal of Hand Surgery*, S0363502323003866. https://doi.org/10.1016/j.jhsa.2023.07.011

Orr, C., Atkinson, R., Ernewein, J., & Tocheri, M. (2023). Carpal kinematics and morphological correlates of wrist ulnar deviation mobility in nonhuman anthropoid primates. *American journal of biological anthropology*. https://doi.org/10.1002/ajpa.24728

Orr, C. M., Leventhal, E. L., Chivers, S. F., Marzke, M. W., Wolfe, S. W., & Crisco, J. J. (2010). Studying Primate Carpal Kinematics in Three Dimensions Using a Computed-Tomography-Based Markerless Registration Method. *The Anatomical Record*, *293*(4), 692-709. https://doi.org/10.1002/ar.21137

Richmond, B. G., Roach, N. T., & Ostrofsky, K. R. (2016). Evolution of the Early Hominin Hand. In T. L. Kivell, P. Lemelin, B. G. Richmond, & D. Schmitt (Éds.), *The Evolution of the Primate Hand* (p. 515-543). Springer New York. https://doi.org/10.1007/978-1-4939-3646-5_18

Stephens, N. B., Kivell, T. L., Pahr, D. H., Hublin, J.-J., & Skinner, M. M. (2018). Trabecular bone patterning across the human hand. *Journal of Human Evolution*, *123*, 1-23. https://doi.org/10.1016/j.jhevol.2018.05.004

Syeda, S. M., Tsegai, Z. J., Cazenave, M., Skinner, M. M., & Kivell, T. L. (2023). Cortical bone distribution of the proximal phalanges in great apes : Implications for reconstructing manual behaviours. *Journal of Anatomy*, *n/a*(n/a). https://doi.org/10.1111/joa.13918

Taleisnik, J. (1976a). The ligaments of the wrist. *The Journal of Hand Surgery*, *1*(2), 110-118. https://doi.org/10.1016/S0363-5023(76)80004-4

Taleisnik, J. (1976b). The ligaments of the wrist. *Journal of Hand Surgery*, *1*(2), 110-118. https://doi.org/10.1016/S0363-5023(76)80004-4

Taquet, P. (2010). 3D imaging applied to palaeontology and palaeoanthropology : The new "pass walls". *Comptes Rendus Palevol*, *9*(6), 255-257. https://doi.org/10.1016/j.crpv.2010.09.003

Tencer, A. F., Viegas, S. F., Cantrell, J., Chang, M., Clegg, P., Hicks, C., O'Meara, C., & Williamson, J. B. (1988). Pressure distribution in the wrist joint. *Journal of Orthopaedic Research*, *6*(4), 509-517. https://doi.org/10.1002/jor.1100060406

Tocheri, M., Orr, C., Larson, S., Sutikna, T., Jatmiko, Saptomo, E., Due, R., Djubiantono, T., Morwood, M., & Jungers, W. (2007). The Primitive Wrist of Homo floresiensis and Its Implications for Hominin Evolution. *Science (New York, N.Y.)*, *317*, 1743-1745. https://doi.org/10.1126/science.1147143

Tocheri, M. W. (2007). *Three - dimensional riddles of the radial wrist : derived carpal and carpometacarpal joint morphology in the genus Homo and the implications for understanding the evolution of the stone tool - related behaviors in hominins,* (doctoral thesis) Arizona State University

Tocheri, M. W., Orr, C. M., Jacofsky, M. C., & Marzke, M. W. (2008). The evolutionary history of the hominin hand since the last common ancestor of Pan and Homo. *Journal of Anatomy*, *212*(4), 544-562. https://doi.org/10.1111/j.1469-7580.2008.00865.x

Tsegai, Z., Kivell, T., Gross, T., Nguyen, N., Pahr, D., Smaers, J., & Skinner, M. (2013). Trabecular Bone Structure Correlates with Hand Posture and Use in Hominoids. *PloS one*, *8*, e78781. https://doi.org/10.1371/journal.pone.0078781

White, T. D., Black, M. T., & Folkens, P. A. (2012). *Human osteology* (3rd ed). Academic Press.

9. ANNEXES

5.1 supplementary data : Carpals frequency histograms

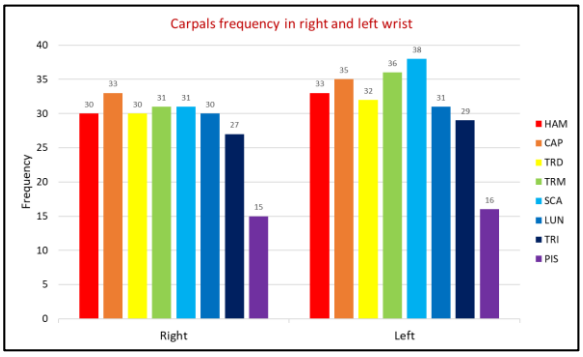

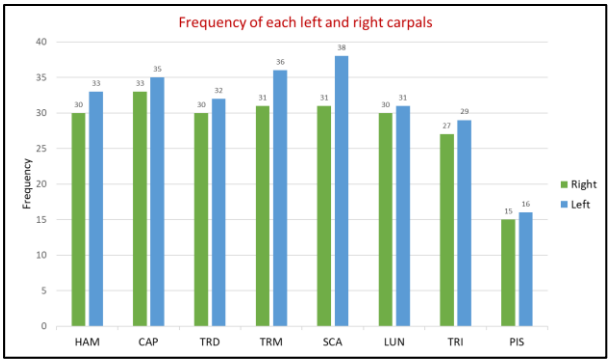

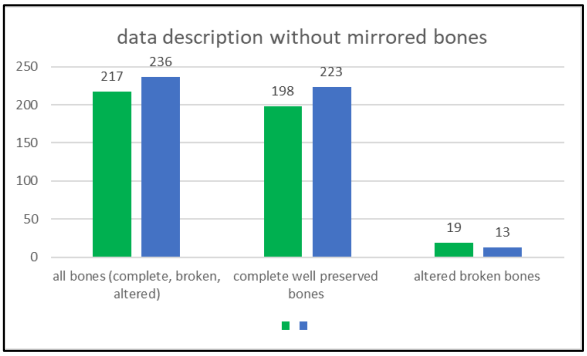

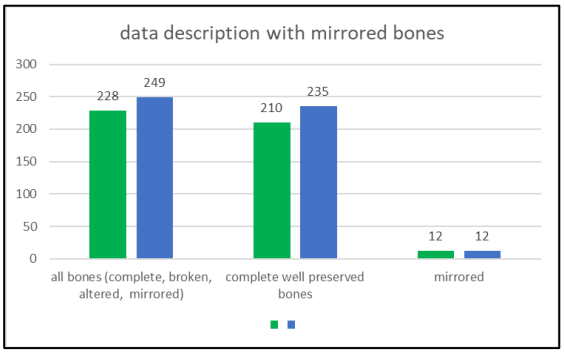

	Pvalue >0,05
TRM	0,084
TRD	0,181
TRI	0,631
CAP	0,631
SCA	0,759
HAM	0,977
PIS	0,714
LUN	0,964

5.1.1 Supplementary data : ANOVA test P value for repeatability test

Table 1 Supplementary : Matrix of pairwise difference in effect size (Zpairwise)

Zpairwise score in wrist (only unmirrored bones)

right

	H1test	H2test	H3test	H4test	H5test	H6test	H7test	No_Modules
H1test		4,18	2,91	3,34	3,12	5,28	2,07	9,04
H2test	4,18		1,41	0,90	1,17	1,42	1,75	6,21
H3test	2,91	1,41		0,49	0,23	2,74	0,56	7,40
H4test	3,34	0,90	0,49		0,26	2,24	0,98	6,81
H5test	3,12	1,17	0,23	0,26		2,52	0,76	7,18
H6test	5,28	1,42	2,74	2,24	2,52		2,85	4,20
H7test	2,07	1,75	0,56	0,98	0,76	2,85		6,17
No_Modules	9,04	6,21	7,40	6,81	7,18	4,20	6,17	

Left

	H1test	H2test	H3test	H4test	H5test	H6test	H7test	No_Modules
H1test		4,17	4,05	3,46	3,11	5,57	2,25	9,21
H2test	4,17		0,03	0,72	1,17	1,86	1,45	6,65
H3test	4,05	0,03		0,67	1,11	1,81	1,39	6,19
H4test	3,46	0,72	0,67		0,43	2,46	0,84	6,88
H5test	3,11	1,17	1,11	0,43		2,91	0,49	7,50
H6test	5,57	1,86	1,81	2,46	2,91		2,84	3,90
H7test	2,25	1,45	1,39	0,84	0,49	2,84		5,89
No_Modules	9,21	6,65	6,19	6,88	7,50	3,90	5,89	

Z pairwise in Wrist* sample (with mirrored bones)

Right

	H1test	H2test	H3test	H4test	H5test	H6test	H7test	No_Modules
H1test		2,86	2,09	2,53	2,31	4,18	1,37	7,76
H2test	2,86		0,83	0,27	0,54	1,64	1,24	6,17
H3test	2,09	0,83		0,53	0,28	2,40	0,53	6,76
H4test	2,53	0,27	0,53		0,25	1,82	0,98	5,89
H5test	2,31	0,54	0,28	0,25		2,08	0,76	6,25
H6test	4,18	1,64	2,40	1,82	2,08		2,55	3,90
H7test	1,37	1,24	0,53	0,98	0,76	2,55		5,70
No_Modules	7,76	6,17	6,76	5,89	6,25	3,90	5,70	

Left

	H1test	H2test	H3test	H4test	H5test	H6test	H7test	No_Modules
H1test		2,44	3,38	2,06	2,20	3,58	1,50	8,18
H2test	2,44		1,05	0,42	0,31	1,35	0,69	7,06
H3test	3,38	1,05		1,46	1,37	0,36	1,56	6,28
H4test	2,06	0,42	1,46		0,12	1,75	0,34	7,42
H5test	2,20	0,31	1,37	0,12		1,67	0,44	7,60
H6test	3,58	1,35	0,36	1,75	1,67		1,80	5,36
H7test	1,50	0,69	1,56	0,34	0,44	1,80		5,88
No_Modules	8,18	7,06	6,28	7,42	7,60	5,36	5,88	

Table 2 supplementary : Matrix of pairwise P value of effect size (Zpairwise)

Right wrist unmirrored N=12								
	H1test	H2test	H3test	H4test	H5test	H6test	H7test	No_Modules
H1test		0,004	0,000	0,001	0,002	0,000	0,038	0,000
H2test	0,004		0,159	0,621	0,816	0,006	0,575	0,000
H3test	0,000	0,159		0,369	0,240	0,156	0,081	0,000
H4test	0,001	0,621	0,369		0,792	0,025	0,328	0,000
H5test	0,002	0,816	0,240	0,792		0,012	0,448	0,000
H6test	0,000	0,006	0,156	0,025	0,012		0,004	0,000
H7test	0,038	0,575	0,081	0,328	0,448	0,004		0,000
No_Modules	0,000	0,000	0,000	0,000	0,000	0,000	0,000	

Left wrist unmirrored N=11								
	H1test	H2test	H3test	H4test	H5test	H6test	H7test	No_Modules
H1test		0,000	0,000	0,001	0,002	0,000	0,024	0,000
H2test	0,000		0,979	0,505	0,269	0,070	0,164	0,000
H3test	0,000	0,979		0,474	0,241	0,063	0,148	0,000
H4test	0,001	0,505	0,474		0,667	0,014	0,400	0,000
H5test	0,002	0,269	0,241	0,667		0,004	0,624	0,000
H6test	0,000	0,070	0,063	0,014	0,004		0,004	0,000
H7test	0,024	0,164	0,148	0,400	0,624	0,004		0,000
No_Modules	0,000	0,000	0,000	0,000	0,000	0,000	0,000	

Right wrist* N=19								
	H1test	H2test	H3test	H4test	H5test	H6test	H7test	No_Modules
H1test		0,037	0,004	0,011	0,021	0,000	0,172	0,000
H2test	0,037		0,405	0,597	0,782	0,017	0,595	0,000
H3test	0,004	0,405		0,785	0,593	0,102	0,214	0,000
H4test	0,011	0,597	0,785		0,803	0,069	0,329	0,000
H5test	0,021	0,782	0,593	0,803		0,037	0,446	0,000
H6test	0,000	0,017	0,102	0,069	0,037		0,011	0,000
H7test	0,172	0,595	0,214	0,329	0,446	0,011		0,000
No_Modules	0,000	0,000	0,000	0,000	0,000	0,000	0,000	

Left wrist* N=20								
	H1test	H2test	H3test	H4test	H5test	H6test	H7test	No_Modules
H1test		0,015	0,001	0,039	0,028	0,000	0,133	0,000
H2test	0,015		0,296	0,678	0,760	0,178	0,491	0,000
H3test	0,001	0,296		0,143	0,169	0,723	0,120	0,000
H4test	0,039	0,678	0,143		0,906	0,080	0,735	0,000
H5test	0,028	0,760	0,169	0,906		0,095	0,658	0,000
H6test	0,000	0,178	0,723	0,080	0,095		0,072	0,000
H7test	0,133	0,491	0,120	0,735	0,658	0,072		0,000
No_Modules	0,000	0,000	0,000	0,000	0,000	0,000	0,000	

Table 3 Supplementary : Total of bones, **Up** are carpals from the distal row, **Down** are carpals from the proximal row.

Distal row					
		HAM	CAP	TRD	TRM
all bones (complete, broken, altered, mirrored)	**Right**	30	33	30	31
	Left	33	35	32	36
	TT	63	68	62	67
altered, broken	**right**	4	3	3	2
	left	5	1	0	4
	TT	9	4	3	6
complete bones unaltered		54	64	59	61
sexe	**Male**	28	32	32	29
	Female	32	35	27	33
mirrored	**Right**	0	0	2	2
	Left	3	1	1	3
	TT	3	1	3	5
unmirrored bones		60	67	59	62

Proximal row					
		SCA	LUN	TRI	PIS
all bones (complete, broken, altered, mirrored)	**Right**	31	30	27	16
	Left	38	31	29	15
	TT	69	61	56	31
altered, broken	**right**	4	3	0	0
	left	2	1	0	0
	TT	6	4	0	0
complete bones unaltered		63	57	56	31
sexe	**Male**	33	29	23	18
	Female	32	26	31	13
mirrored	**Right**	2	4	2	0
	Left	2	2	0	0
	TT	4	6	2	0
unmirrored bones		65	55	54	31